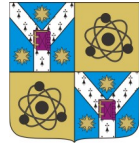




**„AL. I. CUZA” University of Iasi  
Faculty of Physics**



# **Contributions to the study of atmospheric aerosols optical properties using remote sensing techniques**

*PhD Thesis - Summary*

*Candidate,  
Ovidiu-Gelu Tudose*

*Coordinator,  
Prof. Univ. Dr. Dana Ortansa Dorohoi*

Iași – 2013

## **Scientific Committee:**

Prof. Univ. Dr. Sebastian POPESCU

*Committee President*

Faculty of Physics, “Al. I. Cuza” University, Iași

Prof. Univ. Dr. Dana – Ortansa DOROHOI

*PhD Advisor*

Faculty of Physics, “Al. I. Cuza” University, Iași

Prof. Univ. Dr. Sigurd Schrader

*Referent*

University of Applied Sciences, Wildau, Germany

Prof. Univ. Dr. Simion AȘTILEAN

*Referent*

Faculty of Physics, “Babeș-Bolyai” University, Cluj-Napoca

Conf. Dr. Silviu GURLUI

*Referent*

Faculty of Physics, “Al. I. Cuza” University, Iași

## Table of contents

Foreword	1
Chapter I. Basic consideration of laser remote sensing of the atmosphere	4
1.1. The atmosphere – introductory notes	4
1.2. Atmospheric aerosols	5
1.3. Interaction of laser radiation with the atmosphere	8
1.4. The Lidar technique	11
1.5. Lidar Equations and specific parameters	15
1.5.1. Elastic backscatter lidar equation	16
1.5.2. Solution of elastic backscatter lidar equation	19
1.5.3. Solution of elastic backscatter lidar equation obtained using the method of Fernald - Klett	20
1.5.4. Raman backscatter lidar equation	21
1.5.5. Solution of Raman backscatter equation	22
1.5.6. Optical parameters of Lidar technique	23
Chapter II - <sup>ESY</sup> Lidar for atmospheric aerosols – developments and improvements	26
II.1. The elastic backscatter lidar system: <sup>ESY</sup> Lidar	26
II.1.1. Introduction	26
II.1.2. <sup>ESY</sup> Lidar - system Description	27
II.1.3. Matrix formalism for <sup>ESY</sup> Lidar system	44
II.2. The development of <sup>ESY</sup> Lidar	48
II.2.1. The on-axis <sup>ESY</sup> Lidar system configuration	49
II.2.2. Improvements of the alignment module of <sup>ESY</sup> Lidar system	50
II.2.3. Reconfiguration of the reception module of the <sup>ESY</sup> Lidar system	52
II.3. Experimental and computational approaches to optimize the data acquisition of Lidar signals	54
II.3.1. Sources and types of noise in the Lidar technology	54
II.3.2. Optimization and correction methods applied to the Lidar signal	55
II.3.3. Optical alignment of the <sup>ESY</sup> Lidar system	60
II.3.4. Lidar signal validation by direct intercomparison of the <sup>ESY</sup> Lidar system with lidar systems from EARLINET network	62
Chapter III - Applications and data analysis	66
III.1. The development of algorithms used for pre-processing and data-processing	66

III.1.1. Pre-processing of <sup>ESY</sup> Lidar signals	67
III.1.2. Processing of <sup>ESY</sup> Lidar Signals	68
III.2. Assessment of atmospheric aerosols physical properties by Lidar measurements	71
III.3. Experimental case studies - results and discussions	73
III.3.1. Case study – detection of a biomass burning smoke layer (Magurele - Bucharest)	73
III.3.2. Case study - detection of Saharan dust layer (Magurele - Bucharest)	79
III.3.3. Case study - detection of a Saharan dust intrusion episode of the Iasi area	85
III.3.4. Case Study – investigation of the Planetary Boundary Layer (PBL) using the <sup>ESY</sup> Lidar system	88
III.3.5. Case study - analysis of a Saharan dust intrusion episode using complementary techniques (Iasi, Romania)	90
III.3.5. Case study - preliminary experiments using the depolarization module for the <sup>ESY</sup> Lidar system	97
Chapter IV – Optimization of the Lidar system for further applications	100
IV.1. The National Anti-Hail System	100
IV.2. Other Lidar applications	103
IV.2.1. Generating a digital terrain model (DTM) for the Danube floodplain	106
IV.2.2. The study of geomorphological processes on the Danube floodplain	111
Chapter V – Conclusions and perspectives	119
Annexes	122
Appendix 1 - Determination of the overlap function for the <sup>ESY</sup> Lidar system	122
Appendix 2 – Complementary techniques and models used to characterize the atmospheric aerosols	124
Bibliography	134
Personal contributions	145
Acknowledgments	151



# **Chapter I. Basic consideration of laser remote sensing of the atmosphere**

## ***1.1. The atmosphere – introductory notes***

Climate warming is mainly caused by greenhouse gases and manifests itself at a global scale, while local atmospheric cooling can be regionally experienced in the proximity of e.g. industrial sites. Atmospheric aerosols typically cause this effect regional cooling.

The last report of the Intergovernmental Panel for Climate Change – IPCC, 2007, indicates that the contribution of atmospheric aerosols over the total heat exchange balance (Earth - space) is not entirely known. By exploring and quantifying the contribution of atmospheric aerosols to Earth's radiative equilibrium, better climate predictive computer models may emerge, enhancing the understanding of global warming.

Poly-cycle aromatic hydrocarbons and soot emitted by thermal combustion engines (e.g. present in the automotive industry or naturally occurring) part of atmospheric aerosols are of high significant scientific interest since they may produce complex physical-chemical processes in the regional atmosphere leading to weather/climatic changes. The study of different physical-chemical processes in atmosphere having as catalysts aerosols is both done in the laboratory and onsite. In laboratory experiments, the interaction of various chemical compounds adsorbed on the surface of micro-particles of soot, ice and others can be studied. Some of the effects can include carcinogenic effects [1, 2]. By correlating laboratory yielded data with onsite measurements performed over several campaigns (spectral measurements performed from the ground level up to altitudes of 15-20 km), a novel method has been applied at a national level.

## ***1.2. Atmospheric aerosols***

The aerosol is defined as being a system of particles (liquids and/or solids) suspended in a gaseous environment long enough to be observed and characterized. Since in this case the gaseous environment is the Earth's atmosphere, it was convened to name them atmospheric aerosols. In the gaseous atmospheric environment it is common practice to include all solid and liquid particles, except the hydrometeors (water droplets and ice crystals) [3]. In terms of size, the

atmospheric aerosols have a large range, from nanometric particles (a couple of molecules) to particles larger than 10  $\mu\text{m}$ . Aerosols influence the net heat balance received by Earth's crust directly by reflecting the solar radiation back into space and indirectly by modifying the solar radiation absorption and reflection coefficients of the various cloud formations. Equally important, aerosols can act as catalysts for a series of chemical reactions (heterogeneous chemical processes), one example being the chemical reactions leading to the ozone layer thinning. During the wintertime, in the Polar Regions the atmospheric aerosols become larger in size and form stratospheric clouds, polar in origin. Specific chemical reactions create excess reactive chlorine that easily reacts with the ozone in the atmosphere. Similar observations were recorded after major volcanic eruptions (Mt. Piantubo, 1991), which released large quantities of aerosols leading to the thinning the ozone layer [4].

Previous research identified three major atmospheric aerosols that are strongly influencing Earth's climate.

The first type of aerosols is released in major volcanic eruptions (Fig. I.1(a)), being observed in the stratosphere and largely composed of sulfur dioxide compounds. After the volcanic eruptions, the aerosols undergo chemical reactions in the atmosphere where the sulfur dioxide is transformed in sulfuric acid, which may lead to the so-called "acid rain". Atmospheric air streams transport and disperse these aerosols over large regions, sometimes engulfing more than 50% of Earth's total surface. Volcanic generated aerosols can stay in the stratosphere up to two years. They influence the net heat received in the troposphere by reflecting the solar radiation, thus having a chilling-effect. As an example, the Mt. Piantubo eruption led to a drastic Earth cool down (1993) [5].

The second type of aerosol with a significant impact over the climate change, present all-yearlong is the desert dust.

Images provided by weather satellites (Fig. I.1 (b)) show a large number of dust storms originated from Sahara. Typically Saharan dust storms influence the climate of continents (e.g. Europe) and oceans (e.g. Atlantic). Since the dust particles capture solar radiation, the atmospheric layer warms up; this according to recent findings inhibits rain cloud formation, leading to drought periods.

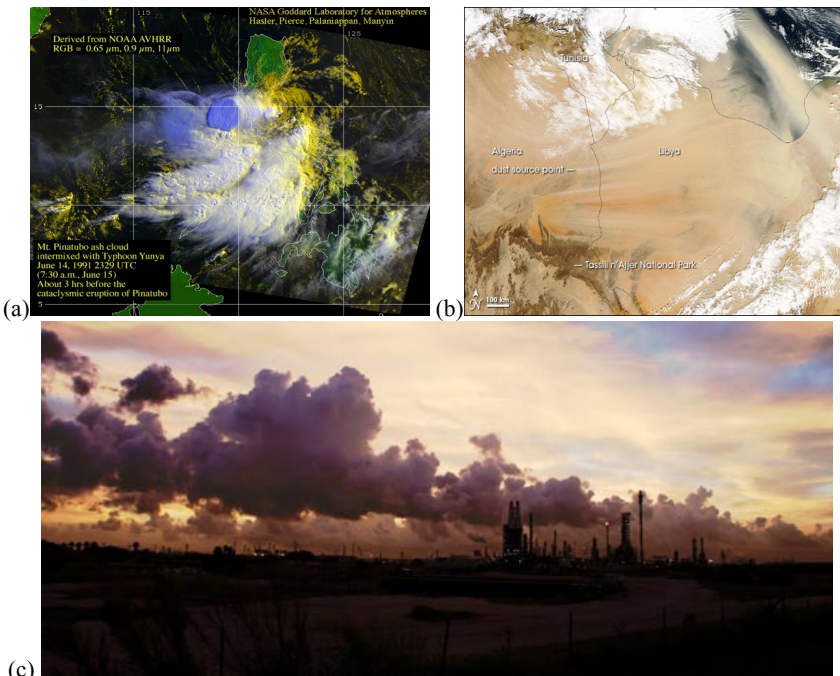


Figure I.1. (a) Volcanic originated aerosols ([http://rsd.gsfc.nasa.gov/rsd/images/Pinatubo\\_huge.jpeg](http://rsd.gsfc.nasa.gov/rsd/images/Pinatubo_huge.jpeg)), (b) Desert dust aerosols (<http://earthobservatory.nasa.gov/Natural-Hazards/view.php?id=16149>), (c) Anthropogenic aerosols (<https://earthdata.nasa.gov/featured-stories/featured-research/regional-pollution-goes-local>).

Anthropogenic, the third type of aerosols (Fig I.1(c)), is typically generated in large industrial areas, or accidentally, namely biomass burning. The anthropogenic aerosols are primarily constituted of sulfates (burning of fossil fuels), carbon particles (biomass burning), etc. The northern hemisphere presents larger concentrations of anthropogenic aerosols due to the intense industrialization. As is the case for the desert dust aerosols, the sulfate aerosols absorb better than reflect solar radiation, leading to a reduction of solar light reaching Earth's crust. Sulfate aerosols have a typical atmospheric lifetime of 3 to 5 days. Additionally, sulfate aerosols influence rain cloud formation by increasing the total number of rain droplets by the reduction of their size. The net effect is that the clouds seeded with sulfate aerosols reflect more the sunlight when compared to regular rain clouds. The lifetime of rainclouds is also increased, thus the total reflected sunlight is higher than the reflected sunlight by "regular" rain clouds.

Presently, an intense and active search in climate forecasting is taken to evaluate the role of atmospheric aerosols interacting with raindrops and rain clouds. Their interaction is rather different than the well-established interaction with greenhouse gases. In addition to the heat radiative effects, the atmospheric aerosols act as seeding centers for cloud formation. Moreover the physical properties (e.g. size) of raindrops are altered [6]. By using the theory of laser depolarization for an initial linear-polarized laser beam, additional information can be gathered over the aerosols geometry.

### 1.3. The Lidar technique

In 1930, E.H. Synge [7] invented a method to characterize the atmospheric density by scattering a light beam, and in 1963 L.D. Smullins and G. Fiocco [8] used for the first time the Lidar system (L*ight* D*etection* A*nd* R*anging*) that employed as a light source a Ruby laser (wavelength 694 nm and energy/pulse ratio of 0.5 J).

Functionally, a Lidar system operates on the same physical principle as the Radar, the main difference is that the source of radiation is a pulsed laser beam instead of the electromagnetic wave used by the more commonly known radar system (they operate at different wavelengths). The wavelength of a Lidar system is chosen accordingly to the atmospheric elements to be investigated, and it can be varied in between 355 nm up to 1064 nm (covering the UV – VIS- IR spectrum) [9].

The pulsed laser beam interacts with the atmospheric constituents and can produce fluorescence, absorption, elastic scattering and inelastic scattering. Part of the backscattered electromagnetic radiation contains information regarding the medium with which it interacted and is captured by the detection system of the Lidar. Typically, additional work is required to separate and weight the contribution of each observed phenomenon to the total possibilities of matter/laser interaction [10, 11].

The Lidar equipment consists of an emission module (including the laser source and the laser expander), a reception module (including among

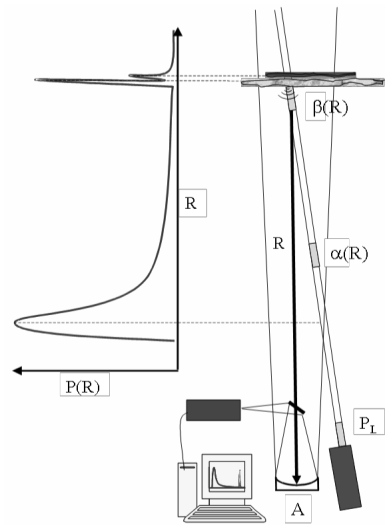


Figure I.2. Operating principle of a Lidar system [13].

others a telescope, lenses, wavelength filters and photomultipliers) and an acquisition system, as depicted in Fig I.2.

The Lidar system is configurable to operate based on various light-matter interactions, thus allowing studying different physical processes (Fig. I.3).

The Lidar system is used to: monitor the degree of atmospheric pollution; verify chemical models of pollution dispersion into atmosphere; weather forecasting (only local and regional); map the physical and chemical state of an ecosystem; or as in our case, quantify the impact of aerosols over the climate change.

In the last years over different regions of the globe, a network of Lidar systems with complementary validation techniques were installed with the aim to study the global climate evolution. Since 2000, EARLINET (European Aerosol Research Lidar Network) network [12] is in charge of monitoring aerosols. In the near future, this network will include the ESYLidar system from Romania.

The Global Aerosol Watch (GAW) program is set in operation to collect experimental data from all the Lidar regional networks and from other complementary networks of instruments (e.g. AERONET (Aerosol Robotic Network) – for technical details see Annex 2). The GAW main purpose is to statistically verify over large periods of time various analytical atmospheric forecasts. In this program, GALION is a new project which aims to group all Lidar systems in a worldwide network thus standardizing operational schemes, the type and the format of acquired data, and finally creating an extensive database of standards and measurements.

The first Lidar system in Romania was installed in 2001 at the National Institute for Research and Development for Optoelectronics. At present there are five operational Lidar stations, all part of ROLINET (Romanian Lidar Network) located in: Magurele (also part of EARLINET), Iasi, Bucuresti Baneasa, Timisoara and Cluj-Napoca. A major interest is to integrate all the Lidar stations part of ROLINET in the global network for atmospheric monitoring. Work is currently ongoing to create and implement a simultaneous measurement schedule for all five stations while using the same algorithms for data processing.

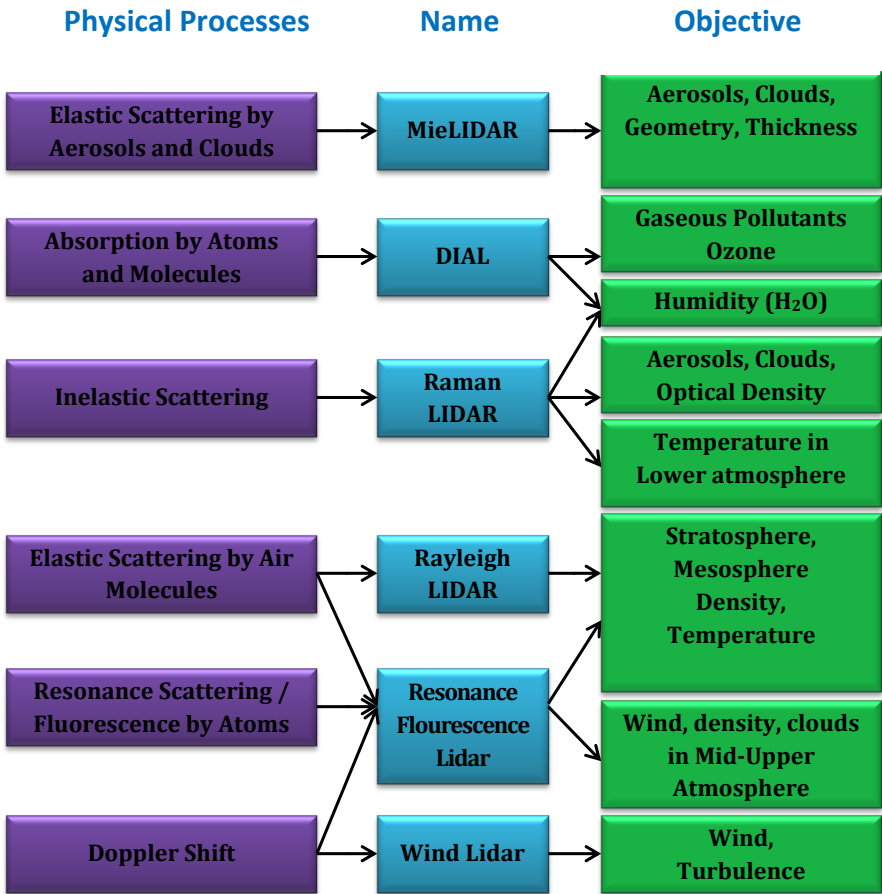


Figure I.3. Types of Lidar systems.

## Chapter II <sup>ESY</sup>Lidar for atmospheric aerosols – developments and improvements

### II.1. The elastic backscattering <sup>ESY</sup>Lidar system

#### II.1.1. Introduction

The <sup>ESY</sup>Lidar system was developed during a research program financed between 2007-2010 by the National Education and Research Ministry, ROLINET (ROMANIAN LIDAR NETwork) (Figure II.1) [13]; partners in this research project being the National Institute for Research and Development for Optoelectronics Magurele, “Al. I. Cuza” University from Iasi, “Babeş-Bolyai” University from Cluj-Napoca, Technical University Timisoara, The National Meteorology Administration, The Regional Center for the Prevention of Major Industrial Accidents Cluj-Napoca and S.C. EnviroScopY S.R.L.



Figura II.1. ROLINET Map  
(The Romanian Network of  
LIDAR systems).

The scientific proposal of the ROLINET project was detailed in the patent filled under the title “Sistem MicroLIDAR pentru detectarea profilelor aerosolilor atmosferici și a norilor 3D”, filled at the State Office for Invention and Trademarks (OSIM) in September 2009 by the National Institute for Research and Development for Optoelectronics Magurele and S.C. EnviroScopY S.R.L. [14]. At present, there are 4 <sup>ESY</sup>Lidar systems, in Iași, Timișoara și Cluj-Napoca between ROLINET.

#### II.1.2. <sup>ESY</sup>Lidar system – technical characteristics and description

The <sup>ESY</sup>Lidar system [15], depicted in Figure II.2 is equipped with the following modules:

- The emission module: the laser source, the laser expander;
- The reception module: telescope, detection optics, photodetectors;
- The acquisition and the analysis module: acquisition card and computer.

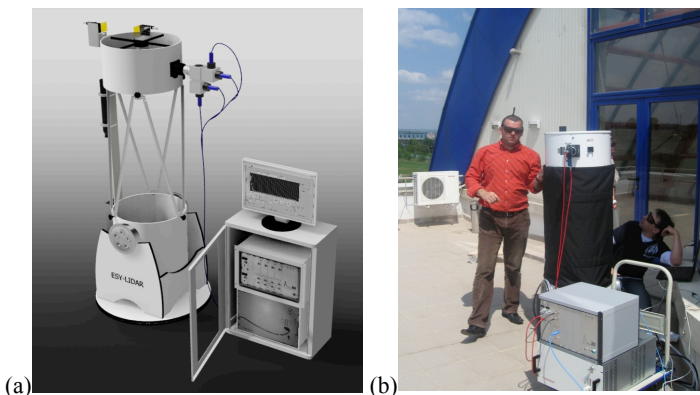


Figure II.2. (a) The <sup>ESY</sup>Lidar system, (b) measurement campaign with the <sup>ESY</sup>Lidar system at the Scientific and Technological Park Tehnopolis, Iasi, 2010.

The schematic overview of the <sup>ESY</sup>Lidar system is depicted in Fig. II.3 (monostatic dual-axis (off-axis) configuration). There are a number of novelties in the <sup>ESY</sup>Lidar setup when compare to other Lidar setups. A patent has been filled with the State Office for Invention and Trademarks (OSIM) by O. G. Tudose, Dr. I. Balin, M.-M Cazacu and A. Bălănici (S.C. EnviroScopY S.R.L.) entitled: “*Configurație de sistem lidar multi-lungime de undă cu aliniere coaxială unică a emisiei laser*” (registry number U/00030/31.07.2013). Briefly, this innovation addresses the new configuration for a Lidar system, namely coaxial emission and Lidar system alignment.

The detection module comprises of a telescope, various optical relevant components (spectrum analyzer, optical collimator elements, spatial filtering) and photodetectors.

The <sup>ESY</sup>Lidar system is equipped with a Newtonian type telescope (MEADE Light Bridge), with the mirror diameter of 16" (406 mm) and a focal length of 1829 mm. The detection module is further equipped with a lens assembly, filters and diaphragms which limit the acceptable spectrum, focus and select the reflected spectrum reaching the photomultipliers to make the most out of the useful signal produces by the laser-matter interaction.

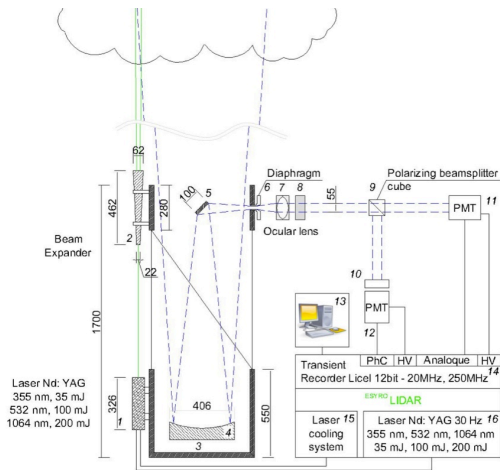


Figura II.3. Schematic overview of the <sup>ESy</sup>Lidar system: 1. Nd:YAG laser source, 2. Laser expander, 3. Newtonian Telescope, 4. Main telescope mirror, 5. Secondary telescope mirror, 6. Adjustable circular diaphragm, 7. Eye-piece, 8. Interference filter, 9. Polarizing beam splitter cube, 10. Optical filter, 11. Photomultiplier (analog mode), 12. Photomultiplier (photon count regime), 13. Computer for data acquisition and analysis, 14. Acquisition board, board for analog to digital conversion and data streaming to computer, 15. Laser cooling unit, 16. Laser power supply.

Recently, an increased interest of the scientific community to find new organic materials (polymers) for dichroic filters is reported. Organic materials present a series of advantages in the fabrication of dichroic filters over the “classic materials” (low manufacturing costs of the thin layers, longer lifetime). These materials may have an active role (select and transmit only a specific light wavelength and suppress over wavelengths, while being less prone to damage by laser radiation) or a passive role (e.g. coating and mechanical damage protection of light optical relevant materials, thus enhancing the lifetime of the optical device) [16, 17, 18]. During a research project conducted at the Technical University of Applied Sciences Wildau, studies were conducted on the properties of these layers of PVV (poly-(p-phenylenevinylene)). The PVV thin layers optical absorption properties were determined with the Lambda 16 Perkin-Elmer Spectrometer and it was determined that it can be used as a material to replace the third polarizing beam splitter cube, being employed to reflect or transmit wavelengths of 532 and 607 nm. Function of thin layer deposition (deposition technique, evaporation rate, activation current, vacuum pressure, bake-out temperature at various temperature of the thin layers), the optical properties can be adjusted to suit the required application.

## II.2. Improvements of the <sup>ESY</sup>Lidar system

During the research period, which resulted in this dissertation, and during other research projects in which I was involved, my contribution lead to:

- A new on-axis configuration for the <sup>ESY</sup>Lidar emission module was developed;
- Improvement of the emission module alignment by replacing the old alignment system with micrometric precision alignment [19];
- Reconfiguration of the detection module to detect three detection channels (532 nm total, 532 nm parallel (analog mode) and 532 nm perpendicular (in photon-counting mode)).

### II.2.1. The on-axis <sup>ESY</sup>Lidar system configuration

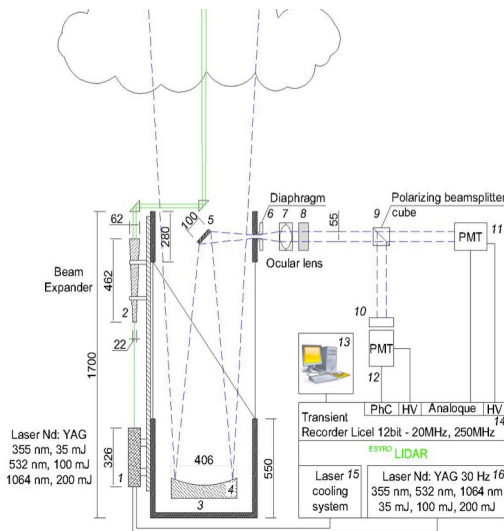


Figura II.4. Schematic overview of the on axis <sup>ESY</sup>Lidar system configuration: 1. Laser source Nd:YAG, 2. Beam expander, 3. Newtonian telescope, 4. Main telescope mirror, 5. Secondary telescope mirror, 6. Adjustable circular diaphragm, 7. Eye-piece, 8. Interference filters, 9. Polarizing beamsplitter cube, 10. Optical filter, 11. Photomultiplier (in analog regime), 12. Photomultiplier (in photon-count mode), 13. Computer for data analysis, 14. Acquisition board, and analog to digital convertor 15. Laser cooling unit, 16. Laser power supply.

Two optical prisms (Thorlabs GmbH) that transfer over 95% of the laser intensity are used to convert the <sup>ESY</sup>Lidar system to the on-axis configuration (Fig. II.4). A large reflection coefficient attenuates the laser

probe, thus reducing the intensity of the useful Lidar backscattered signal. To reduce the transmission loss, it was proposed to coat the two prisms with thin material layers that may improve the transmission coefficient. Function of the materials used (e.g. organic materials) for thin film coating under controlled atmosphere (ultra high vacuum, specific temperature and controlled deposition rate), optical prisms with a reflectivity of up to 99.999% may be obtained. Also function of the physical and chemical properties of the organic material of choice, the selectivity of the transmitted wavelength through the prisms can be further enhanced. By depositing such organic thin films, a new type of mirrors is created, the so-called dielectric mirror (Bragg mirror) which function based on the interference of light reflected from different layers of the dielectric stack. Various studies [20, 21, 22] propose deposition and characterization methods for polymer thin film coatings. As a part of the research conducted at the University of Applied Sciences Wildau, Germany, I investigated thin layers of PTFE (polytetrafluoroethylene), an organic material with exciting physical and chemical properties [23]. The morphology of the thin films of PTFE deposited under ultra high vacuum where the deposition rate, the deposition temperature, and the activation current were varied was investigated. Thus, the molecular structure of the thin layers was researched with IR-spectroscopy; the refractive index was investigated by ellipsometry while the morphology was characterized by atomic force microscopy. As an outlook, of high interest is to deposit such organic thin layers on the optical prisms of the on-axis <sup>ESY</sup>Lidar system to improve the radiation reflectivity to values of at least 99%.

### **II.2.2. Improvements of the alignment system**

Before the upgrade of the alignment system, the emission module (laser and the laser beam expander) was being aligned by stands that had 6 degrees of freedom with mm precision (Fig. II.5.(a) and (b)). During the research project detailed in the doctoral dissertation, a new fixation/alignment system was developed. It features 4 micrometric stands manufactured by Thorlabs GmbH that allow high-precision alignment, while preserving the six degrees of alignment required for the emission module.

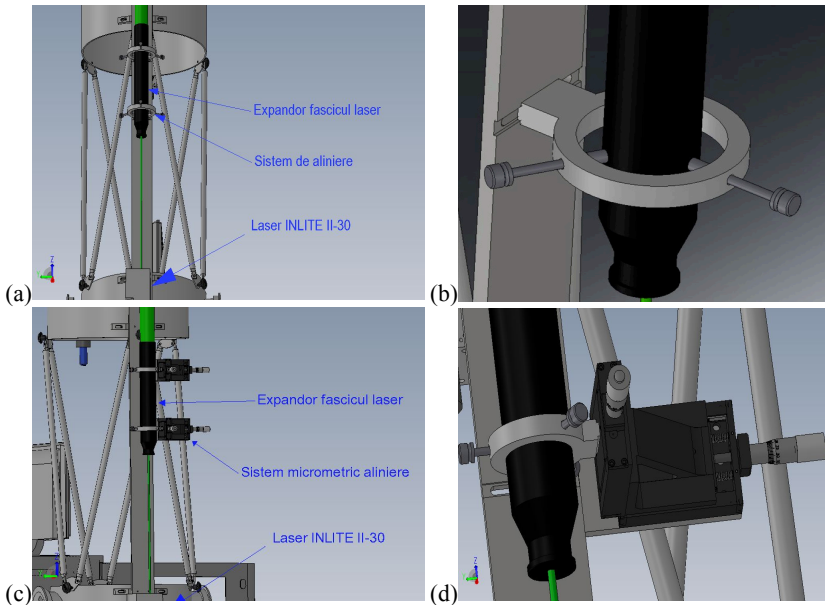


Figure II.e. (a) Overview of the alignment system and (b) detailed view of the “classic” fixation/alignment system for the emission module c) Overview of the alignment system and (d) detailed view of the micrometric fixation/alignment system for the emission module.

By upgrading the fixation/alignment system a decrease of the distance between the main optical axis of the emission module and the main axis of the telescope (from the initial 360 mm to 320 mm). This reduced distance changes the overlap factor of the Lidar system, factor describing the overlapping radiation ratio at emission and reception. According to previous works [9, 24, 25] and Annex 1, the overlapping factor is of uttermost importance since is a constant in the Lidar equations (described in Chapter I of the Doctoral Dissertation).

A LabVIEW code developed based on the equations summarized in Annex 1 [9, 16] and on the technical specifications of the emission module and telescope is used to simulate the overlapping factor of the Lidar system. As further modeling parameters, the overlapping factor can be computed function of the distance between the two aforementioned optical axis, and the declination angle between axis for a given optimal configuration at which the Lidar signal is acquired.

Table II.5. Required parameters for computing the overlapping factor of the Lidar system

Parameter	<i>ESY</i> Lidar – standard configuration	<i>ESY</i> Lidar – upgraded configuration
Laser pulse energy [mJ]	100	
Telescope object diameter [mm]	40	
Multiplication factor of the laser beam expander	5x	
Initial laser divergence [mrad]	0.75	
Distance between axis [mm]	360	320
Diameter of the Diaphragm aperture [mm]	11	
Declination angle between axis [mrad]	0.45	0.43

By computing the overlapping factor using the values give in Table II.5, it is noticed that a value of 1 is achieved at an altitude of about 750 m (in the standard configuration) [16, 26] and 700 m (in the upgraded configuration), meaning that the laser beam enters the field of view at the same distance, see Fig. II.6.

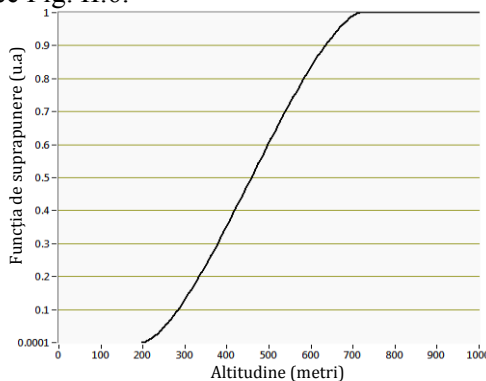


Figura II.6. The overlapping function characteristic to the *ESY*Lidar system.

The circular diaphragm located in the reception module can be reduced in size during sunny and bright days (necessary to maintain a good signal to noise ratio at the) and to maintain the photomultipliers in the linear response region for the wavelength of interest. By modifying the circular diaphragm, the overlapping factor is changing. To preserve the correct Lidar signal the declination angle has to be adjusted. Accordingly, for a variation of the diameter of the diaphragm from 12 mm to 3 mm, the declination angle has to be changed from -0.5 mrad to 0.35 mrad (the minus sign denotes the declination orientation), thus the altitude where the overlapping factor becomes 1 can vary between 700 and 950 m.

### II.2.3. Reconfiguration of the reception module of the <sup>ESY</sup>Lidar system

In order to succeed depolarization studies receiver module contains a polarizer cube (to determine the particles sphericity from atmosphere, thus making a distinction between clouds (cirrus clouds) that containing ice particles, passing only particles containing water (cumulus nimbus type), other types of aerosols (volcanic ash, mineral dust, urban, etc.)), (Figure II.7).

This Lidar technique consists in the emission of a linear polarized laser beam (parallel polarized by convention) and the detection of both backscattered laser radiation components (parallel and perpendicular) with the means of a beam splitter cube.

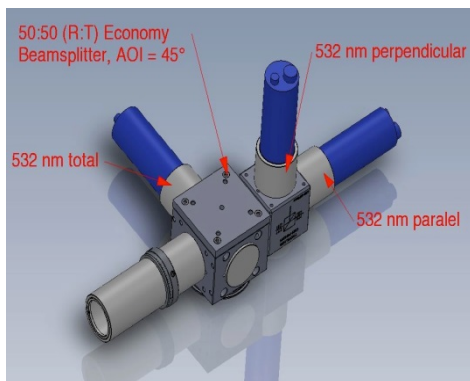


Figure II.7. <sup>ESY</sup>Lidar reception module for depolarization studies

Qualitative results indicate the capability of atmospheric aerosols to rotate the polarization vector of the laser probe. As an example, an ice particle (low asphericity) has a depolarizing degree of 30-40% while a water droplet has a significantly lower depolarizing factor of only, 2-3% [27].

Typically the perpendicular component at the optical axis of the backscattered radiation is a very low intensity component and it is measured with a photomultiplier working in photon-counting mode while the parallel polarized component is measured in by another photomultiplier acquiring in analog mode.

Processing the two different signals given by the photomultipliers is rather complex and prone to measurement errors (especially the photomultiplier set in photon count mode since the quality and stability of the discriminating electronics is essential). To reduce the measurement errors, the reception module was reconfigured and additionally, the depolarizing Lidar measurements were simplified.

With a beam splitter (50:50) manufactured at Thorlabs GmbH, placed in front of the polarizing cube, we measure the backscattered radiation at a wavelength of 532 nm (total), and the two perpendicular polarized components (parallel (analog mode) and perpendicular (photon-count

mode)). In Chapter II of this Doctoral Dissertation it will be shown that this new reconfiguration of the Lidar system was implemented and tested. Preliminary results are promising, indicating a reduction of measurement errors. An immediate upgrade can be implemented on all the Lidar systems from the ROLINET network.

### ***II.3. Experimental and computational methods developed to optimize the data acquisition of Lidar signals***

#### **II.3.1. Sources and types of noise in Lidar technology**

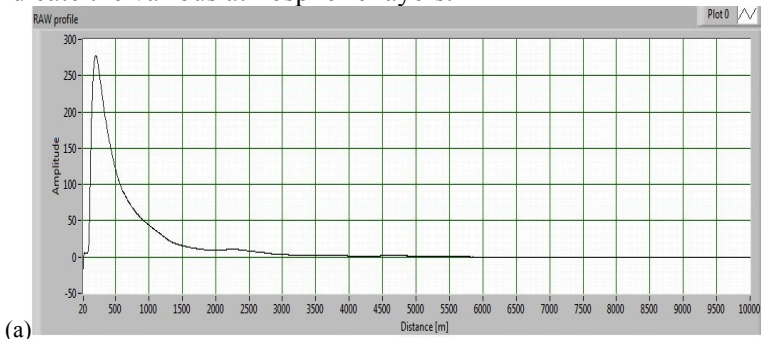
The Lidar signal arriving at the acquisition board is an electrical signal emerging from the conversion of light by photomultipliers located in the detection module. The characteristics of this electrical signal contain all the relevant information resulted from the laser-atmosphere interaction. Any source of measurement errors must be accounted for, and reduced if possible.

The largest contributions to measurement errors are the background radiation and the dark current [24]. Other noise source is the electronic noise (thermic noise, 1/f noise and impulse noise). This subchapter explores means of noise reduction.

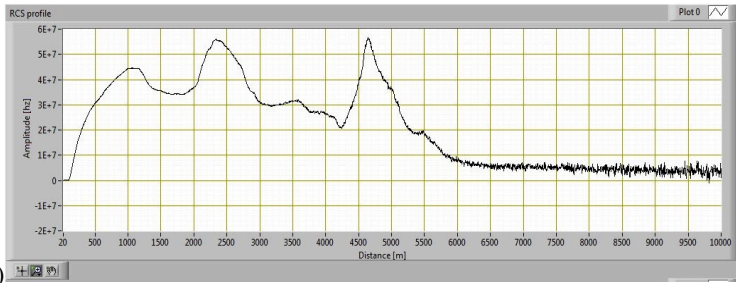
#### **II.3.2. Optimization and correction methods applied the Lidar signal**

##### Distance correction

Figure II.8 (a) shows a typical raw Lidar measurement (532 nm, analog mode). To this raw signal we will apply the correction and optimization methods. The amplitude of the atmosphere backscattered Lidar signal varies with the altitude, the higher the altitude, the collected amplitude is smaller. To normalize for this, the Range Corrected Signal (RCS) is defined as the product between the amplitude of the Lidar signal and the distance squared. The RCS profile is shown in Fig. II.8(b), and it can indicate the various atmospheric layers.



(a)



(b) Figure II.8. (a) Raw Lidar signal and (b) Range corrected signal Lidar (29.05.2013, 20.40 – 21.00 LT).

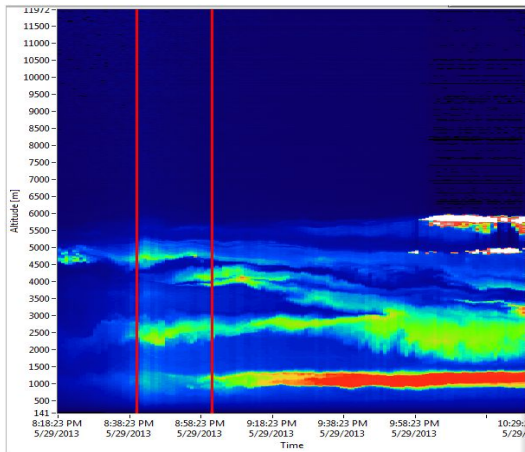


Figure II.9. Lidar – range corrected signal - 29.05.2013, 20.40 – 21.00 LT.

### Dark current/noise correction

To correct for dark current/noise created by electronic components, before any set of atmospheric measurements, a 5 minutes run and record of noise is performed. The Lidar system will have the main optical mirror closed and the photomultipliers will not collect any photons.

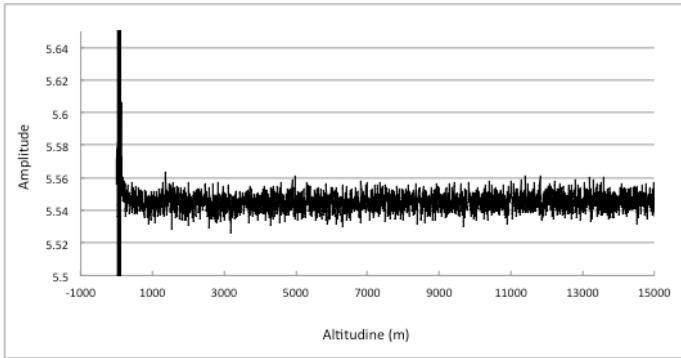


Figura II.10. Dark current/noise measurement (29.05.2013, 21.00 LT).

Electronic oscillations (easily observable in fast Lidar measurements) are caused by electronic noise from: the triggering system, the reflections from the near vicinity of the telescope, and from the Lidar signal arriving from various sources located along the laser beam path (e.g. clouds). To reduce this effect, the detection module (Licel) is used. The module is optimized to work with Lidar signals of up to 100 mV. Neutral optical filters can be used if stronger Lidar signals are required (in the Volt range). As an example, the intense peak in amplitude observable in Fig. II.10 is caused by a secondary reflection of the laser beam in the proximity of the telescope.

### II.3.3. The optical alignment of the <sup>ESY</sup>Lidar system

#### The telecover method

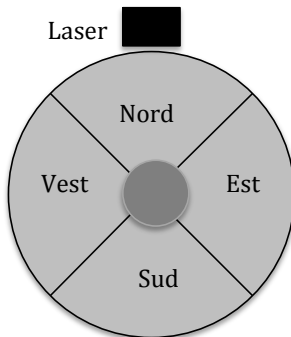


Figure II.11. Telecover method - the relative position of four areas to the laser axis [28].

The telecover method, detailed by V. Freudenthaler [28], was used to check the optical alignment of the <sup>ESY</sup>Lidar system. This method states that any Lidar signal collected in any of the 4 hypothetical main mirror zones (Fig.II.11) should have the same shape independent of collection zone. This method can be applied for the Lidar system in mono-axial configuration, and also for the Lidar system in bi-axis configuration that employ Cassegrain or Newtonian telescopes. The optical alignment of all Lidar systems included in EARLINET is the telecover method.

To perform the telecover method the following steps should be done:

- Split the main mirror in 4 quadrants, according to II.11;
- Cover 3 out the 4 quadrants and acquire the Lidar signal and save the file;
- Repeat the previous step until all 4 quadrants are mapped.

To verify the alignment of the Lidar system, the first record from the North, followed by the signals from the East and West zones and, finally, the signal coming from the South were take into account.

An example of the <sup>ESY</sup>Lidar signals collected from the 4 zones is given in Fig II.12.

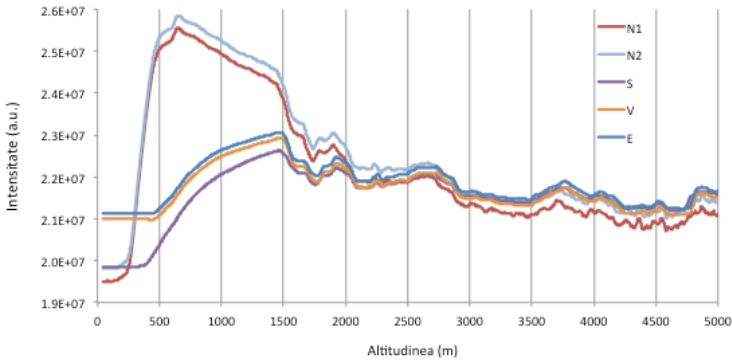


Figura II.12. The telecover method – The Lidar signals recorded in the 4 zones of the telescope[28].

The telecover method is easy and fast to apply, does not depend on the construction of the Lidar system and does not require any additional information. In the acquired spectrum, an experienced user might further observe misalignments of the following components: laser source, telescope, and diaphragm. Optical inhomogeneity might arise from spatial inhomogeneity of optical elements or varying optical transmission coefficients (e.g. interferential filter, beam expander) and even photodetectors inhomogeneity [20].

The acquisition time has been 1 minute for each Lidar signal, while the first are N1 (Fig.II.12) has been measured again (N2) to check if the atmosphere has changed significantly during the measurements.

### Rayleigh fit

WE use the Rayleigh fit (software feature) to optimize the Lidar signal to allow data handling and interpretation [24, 29]. The theory behind the Rayleigh fit is described in Chapter I of this dissertation. The Lidar

equation must be solved for molecular backscattering. Since the molecular backscattering coefficient is function of the molecular concentration over the altitude, to obtain the Lidar molecular profile information over temperature and pressure must be known. To obtain the temperature and pressure profiles over the altitude first we record the temperature and pressure at ground level. The data is recorded with a weather station, model Davic Vantage Pro 2 Plus (T=18.2 °C and P=1016 hPa) [25].

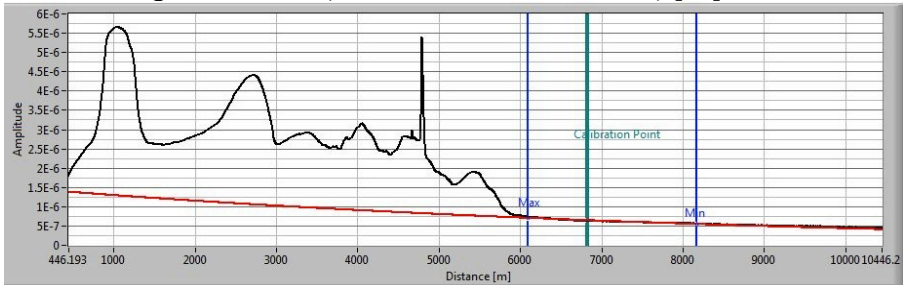


Figure II.13. Rayleigh fitted and optimized Lidar signal.

For the <sup>ESY</sup>Lidar system we considered a homogenous atmosphere at altitudes between 6000 and 8000 m, and the calibration altitude was set at 6900 m. Observable in Fig. II.13 the Rayleigh fit (red line) and the theoretical model match in the 6000 – 8000 m range.

## Chapter III – Lidar application and examples

### III.3. Case studies – results and discussion

#### III.3.1. Case study – smoke detection from biomass burning (Măgurele – București)

Biomass burning (green or dry) ejects large quantities of particles (mainly carbon) and gasses, including greenhouse gases. In the period 11th of July 2012 23.33 UTC – 12th of July 2012, 00.03 UTC, a well defined smoke layer was detected and registered by the RALI system at an altitude of 2500 m. This layer was detected on the channel 1064 nm (Fig. III.1(a)) and on the 532 nm channel (Fig. III.1(b)).

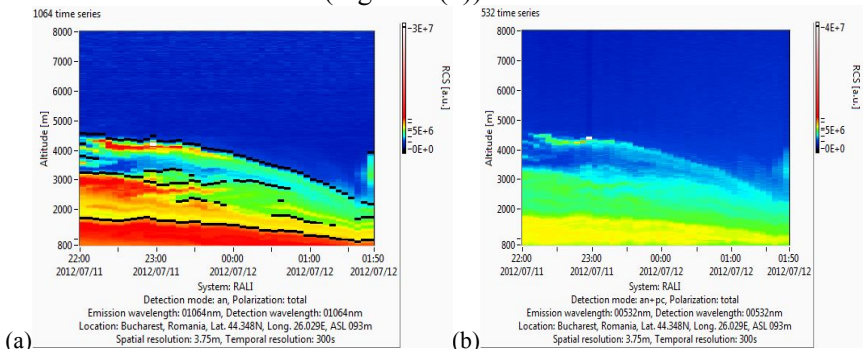


Figura III.1. Vertical and temporal distribution of aerosol layers (11 - 12 July 2012): a) detection at 1064 nm and b) detection at 532 nm (Range corrected Lidar signals).

By applying the Tesche method [30], the vertical profiles (Fig.III.6) for the backscattering and extinction coefficients of the polarizing and non-polarizing particles are obtained. For dust, an average value of polarization of 30% was used while for smoke the value was considered 3%. The average characteristic value of the Lidar ratio was considered 30 sr for dust and 80 sr for smoke. The vertical atmospheric column is characterized by a mix of smoke (non-polarizing) and dust (polarizing), each contributing differently to the backscattering and extinction coefficients. Interesting to notice is the fact that although the backscattering coefficient is rather similar up to about 5000 m, the extinction coefficients are different. This observation is explained accounting for the fact that the absorption coefficient for the smoke particle is significantly larger than for dust. Figure III.2 (c) depicts the atmospheric mass concentration profiles for dust (black line), smoke (red line) and aerosols (green line).

Tabel III.1.

Aerosol Type	Main components	Ratio
Desert dust (non-polarizing particles)	Minerals (transported)	0.1
	Minerals – nucleation mode (mixture quartz and dust)	0.1
	Water soluble (sulfates, nitrates & others)	0.9
Smoke (non-polarizing particles)	Water soluble	0.5
	Smoke (black carbon)	0.5

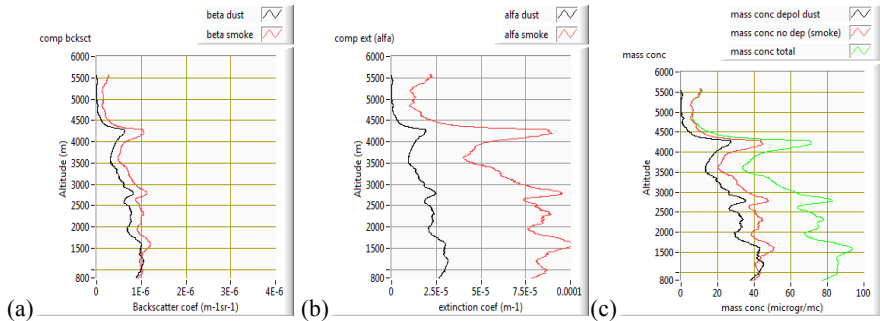


Figure. III.2. EMAP/Pegasus Campaign - 11 July 2012 (23.32 UTC) – 12 July 2012 (00.02 UTC): (a) Vertical backscattering profile, (b) extinction and (c) mass concentration for polarizing particles (black line) and non-polarizing particles (red line). The total mass concentration is depicted in green.

These profiles were obtained by multiplying the extinction coefficients (Fig III.2 (b)) with the efficiency mass extinction for dust ( $0.4 \text{ m}^2/\text{g}$ ) and smoke ( $0.5 \text{ m}^2/\text{g}$ ). The values for the efficiency mass extinction were taken from the OPAC model, under the assumption of relative humidity of 50%.

From Figure III.2 (a) it can be concluded that an almost equal amount of dust and smoke are present up to 1300 m. Traffic and construction sites mainly produce the dust particles closest to the ground level. The composition of the dust generated at the ground level mainly contains minerals, but also organic matter (micro-organisms). The smoke (small particles, highly absorbing) is almost always present close to the ground level due to various sources of fuel combustion (cars, industry, etc). The ratio dust to smoke may vary based on the anthropic seasonal activities and local weather conditions.

In the troposphere the smoke/dust concentration is no longer influenced by local sources but it is mainly governed by long-range transport. For the above presented data, the layers between 1300 m and 4500 m are characterized by a high content of smoke particle, fact verified

by the solar photometer (technical details in Annex 2) (Fig. III.3 (a)) and with the RALI system.

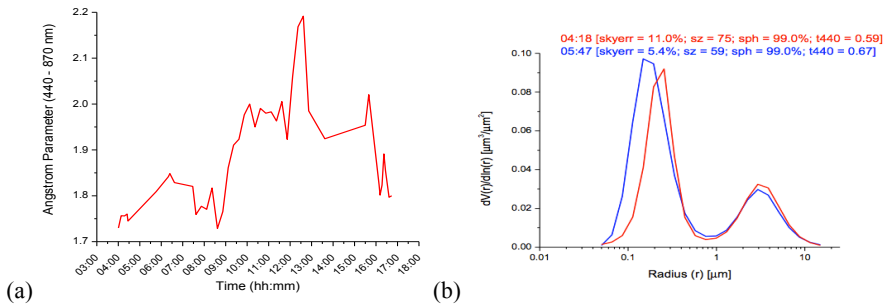
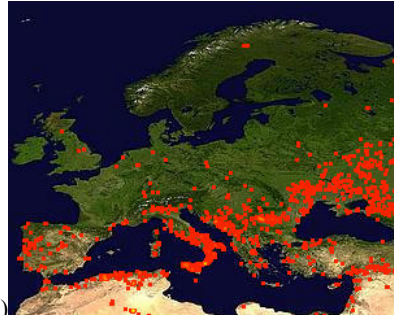
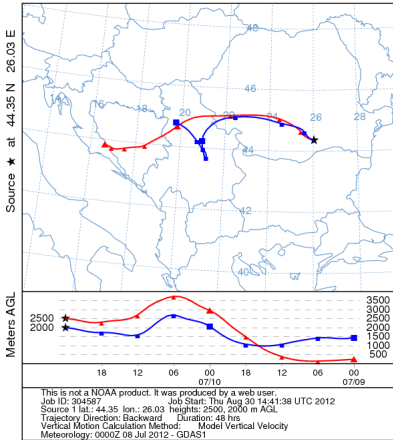


Figure III.3. (a) The variation of the Angstrom parameter and (b) the average variation of particle size as measured with the solar photometer (Măgurele, 11 July 2012 – 12 July 2012).

The increase in the Angstrom parameter (Fig III.3(b)) indicates the arrival (09.00 UTC) of the aerosols in the local region. At midnight an average value for the layer of  $1,8 \pm 0,3$  was determined by Lidar. The high value of the Angstrom parameter indicates the presence of small particles, result in agreement with the size distribution measured with the solar photometer used at different wavelengths (Fig. III.3 (b)). The size distribution of the larger particle is also plotted in the same figure, corresponding to a low dust content.

Based on the HYSPLIT models (Fig. III.4 (a)) and MODIS (Fig. III.4 (b)) we can confirm that these types of aerosols are a mixture of smoke (predominant) and dust. The trajectories of air masses in the troposphere reaching Magurele originated in Southern Europe, where MODIS indicates (red dots) a high density of woods burning. These air trajectories originate at low altitude and do not encounter rain in their path. It is very likely that these smoke particles mixed with other pollution generated aerosols are detected at Magurele.

NOAA HYSPLIT MODEL  
Backward trajectories ending at 0000 UTC 11 Jul 12  
GDAS Meteorological Data



(a) HYSPLIT trajectories 11 July 2012; (b) Fire map MODIS (10 days).

BSC-DREAM8b Dust Loading (g/m<sup>2</sup>) and 3000m Wind  
60h forecast for 00UTC 12 JUL 12

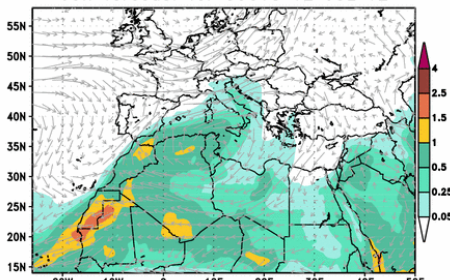


Figure III.5. DREAM Forecast for July 11, 2012 and 23:00 UTC - July 12, 2012, 00:00 UTC.

In the period 11th July 2012 – 12th July 2012, the DREAM model does not confirm the presence of Saharan dust over Romania (Fig III.5), but confirms the presence of mineral dust in the Southern Europe, thus explaining the presence of a small concentration of polarizing particles at the measurement site. These particles are mixed with smoke particles.

### III.3.2. Case study – Saharan dust detection at Măgurele – Bucharest

According to studies made up to now the Saharan dust is the largest source of mineral dust [31] to and over Europe. It is a seasonal event and the highest frequency of detecting Saharan dust is the period February - June and October – December [32]. Yet, Saharan dust intrusion can be detected all along the calendar year. Due to the large distance between Romania and Saharan, the Saharan dust is typically mixed with other particles (e.g. originated from European continental pollution or smoke). As a consequence the optical properties of mineral dust do not coincide

with the properties of pure Saharan dust, although those particles are hardly reactive and hygroscopic.

A typical event of Saharan dust intrusion was recorded during 15th of July 2012. The presence over Romania of dust formations originated from Sahara is confirmed by the HYSPLIT trajectories (Fig. III.6 (a)) and the forecast given by the DREAM model (Fig. III.10 (b))

The RALI system detected over the region of interest the dust (Fig. III.7 (a) showing the Lidar 1064 nm) and the degree of volumetric polarization is computed (recorded at 532 nm) and depicted in Fig. III.7 (b). Noteworthy, the layer located at the altitude between 2500 and 5000 m is characterized by strong polarization, phenomenon characteristic to Saharan dust.

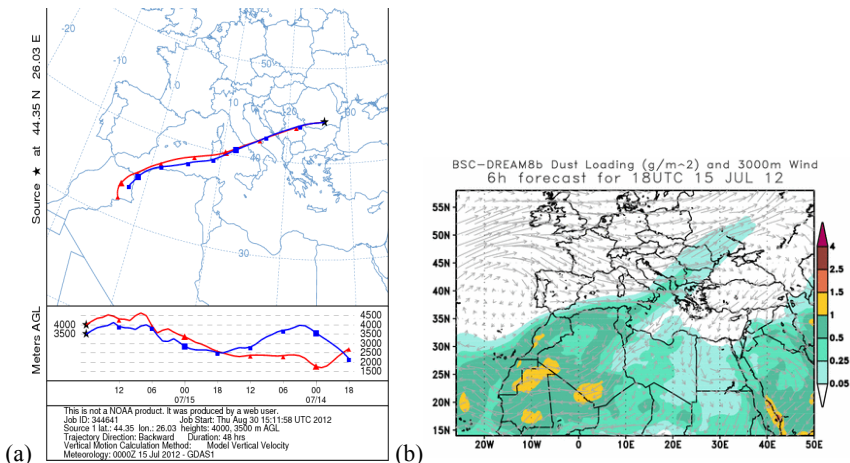


Figure III.6. Aerosols sources during 15th of July 2012: (a) HYSPLIT trajectories; (b) DREAM model forecast.

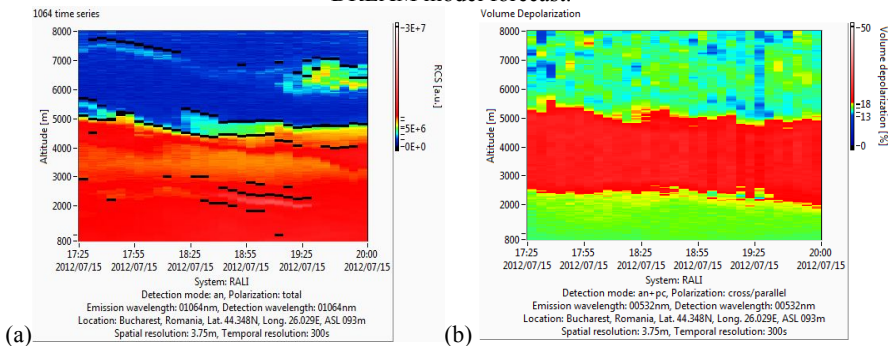


Figure III.7. Vertical and temporal distribution of aerosol layers during 15th of July 2012: (up) distance corrected signal 1064 nm and (down) volumetric polarization at 532 nm.

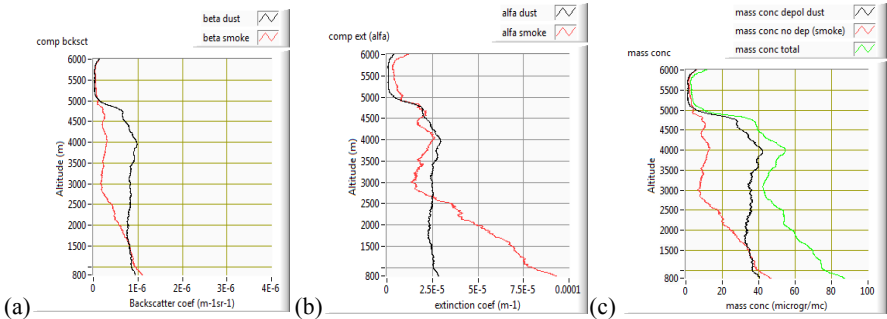


Figure III.8. EMAP/Pegasos - 15 July 2012 (18:00 UTC - 19:00 UTC): (a) Vertical profiles of backscattering, (b) extinction and (c) mass concentration for polarizing particles (black line) and non-polarizing (red line). Total mass concentration depicted in green.

As in the previous case study, by applying the Tesche method we deduce the vertical profile for the backscattering coefficients and extinction for both polarizing and non-polarizing particles (Fig. III.8 (a) and (b) and the mass concentration profile (Fig. III.8 (c)).

A quantitative validation for the dust concentration profile was performed by estimating the total atmospheric dust column, by accounting an average mass concentration of  $35 \mu\text{g}/\text{m}^3$  up to a height of 5000 m and a zero value above the specified height (Fig. III.8 (c)). The value of  $0.175 \text{ g}/\text{m}^2$  is in good agreement with the range calculated by DREAM for Romania ( $0.05 - 0.25 \text{ g}/\text{m}^2$ ) with higher values in Southern Romania, Figure III.6 (b).

As in the previous case, the dust and smoke concentration close to the ground level is almost the same, originated mainly from local sources. At an altitude larger than 1500 m, the concentration of fine particles (smoke) decreases exponentially, while the dust particle concentration increases up to an altitude of 5000 m. The dust layer is clearly visible in the backscattering profiles (Fig. III.8. (a)) but not visible in the extinction profile (Fig. III.8 (b)). Accounting that the mineral dust is strongly scattering and only weakly absorbing can explain this observation.

The Angstrom coefficient measured with the RALI system is small at altitude of 2000-3500 m, when compared to the close to ground atmosphere ( $1.7 \pm 0.3$  up to 2000 m, and  $0.8 \pm 0.2$  above 2000 m). The reported values are verified with the solar photometer.

In conclusion, the method proposed by Tesche combined with the OPAC model was successfully applied to determine the mass concentration by means of optical techniques. By using additional information provided by complementary techniques (e.g. solar photometer) or other models

(HYSPLIT, DREAM, MODIS) we can identify the nature of the aerosol layers.

### III.3.3. Case study- Saharan dust detection at Iași

In this case study we present the intrusion of mineral aerosols of Saharan origin in troposphere during the period 29 – 30 May 2013. The Lidar measurements were performed in the Laboratory for the Optics of Atmosphere, Spectroscopy and Lasers (GPS coordinates 47.19N 27.55E 175.0 ASL).

As a complementary technique, the atmosphere was monitored with satellite imagery, using the RGB product (channels IR8.7, IR10.8 and IR12.0) (technical details in Annex 2) to detect mineral dust. Forecast methods were also employed, such as GFS and ECMWF (by EUMETRAIN) (technical details in Annex 2). Dedicated models for Saharan dust intrusion forecasting such as DREAM, solar photometry, HYSPLIT, and weather balloons provided trajectory mapping.

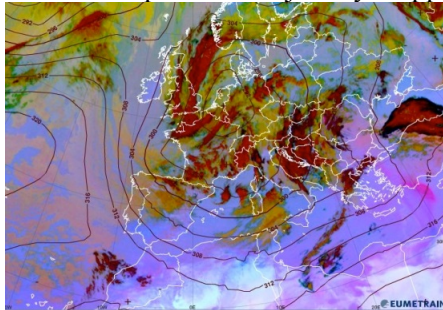


Figure III.9. EUMETRAIN-geopotential field at 700 hPa, apply to Dust RGB satellite images (IR8.7, IR10.8 and IR12.0).

Lidar data pre-processing (according to paragraph III.1.1) allowed the identification of Saharan dust at the location of the Lidar system. The Synoptic background in Europe facilitated the spread of the Saharan dust over the region of interest. The atmospheric models forecasted a wind direction that enabled the transport of Saharan dust over the Iasi region. The DREAM model, dedicated to forecast Saharan dust intrusion, indicated that at 18.00 UTC on the 29<sup>th</sup> of May, the Saharan dust would reach Romania.

With satellite imagery, the Saharan dust was visualized entering Romania from the South/South-West direction. The meteorological conditions allowed the dust storm to encompass the whole Romanian territory.

Lidar data confirmed the presence of Saharan dust at altitudes of 1500 m, respectively 5000 m (Fig. III.11), while the HYSPLIT model indicates the trajectories of the Saharan dust from origin to the location of the experiment.

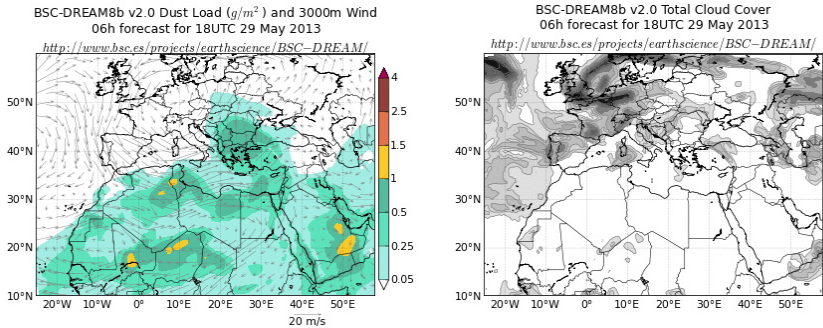


Figure III.10. The DREAM model – forecast for the dust quantity ( $g/m^3$ ) and wind (at 3000 m), left hand side image and the nebulosity forecast, timestamp 29 May 2013 18.00 UTC.

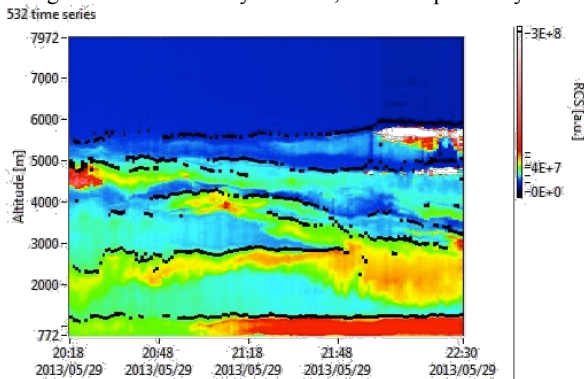


Figure III.11. Distance corrected Lidar data, channel 532 nm analog mode, temporal resolution 1 minute, spatial resolution 3.75 m, 29 May 2013.

In conclusion, we forecasted by using the available models the intrusion of Saharan dust storms over the territory of Romania. Lidar data enabled the characterization of the Saharan dust, namely altitude and the geographical area where it was most dense. The trajectory of the Saharan dust where simulated with HYSPLIT, a good agreement being reached between modeling and experimental data.

### III.3.4. Case study – Investigations of the Planetary Boundary Layer using the <sup>ESY</sup>Lidar system

The Planetary Boundary Layer (PBL) is the inferior layer of the atmosphere and is directly influenced by the processes that take place at the surface of the Earth. Some of the most important meteorological processes take place in this layer, such as: evaporation, raining, snowing, and cloud formation. It is important to study the PBL since the average daily altitude and its rate of climb are not constant, varying function of region, weather and period of time. Most often, the upper limit of the PBL is not well defined. The mix between the PBL and the troposphere (next atmospheric layer) is occurring during the daily rise or fall of the PBL, while the interaction layer is defined by a strong thermal inversion. The altitude of the inversion layer is low above sea and oceans and rises up to 3000 m above continents. The relative heat at the surface of the Earth causes the creation of a Mixt Layer (ML) in the interior of the PBL, which is always present during the day, while at night, disappears leaving behind a Residual Layer (RL) above a Stable limit Layer (SL) with an altitude of a couple of hundreds of meters [33, 34].

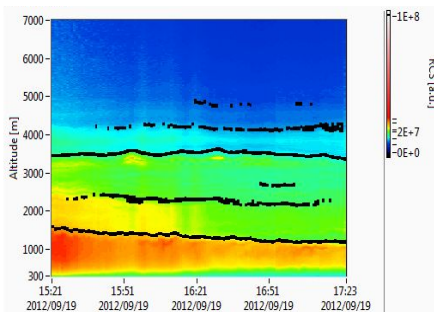


Figure III.12. Representation of changes in the planetary boundary layer (19/09/2012, Iași, Lidar measurements campaign AQUA-GRO).

Since the distance corrected Lidar signal is directly proportional with the intensity of the aerosols backscattered radiation, the data representation allows a direct quantitative analysis of the vertical distribution of aerosols and their temporal evolution (Fig. III.12). Furthermore, the daily evolution of the PBL can be monitored over various weather conditions.

In September 2012, part of ROLINET, a measurement campaign (entitled AQUA-GRO) was done by all Lidar station from Romania. The measurements were carried out according to a standard procedure. During the above-mentioned campaign, the PBL was also monitored.

In Figure III.12, it can be observed the variation of the PBL between 1000 and 2000 m in a time frame of about two hours. Thin layers of aerosols in various concentrations are noticed in the superior layers. Most likely those aerosols are of Saharan origin (mineral dust). During the night

the PBL becomes more visible since the background noise is lower and the fewer anthropogenic activities are present than during the daytime [35]. The mixture between the PBL and the troposphere occurs during the daily rise and fall of the SL.

#### **III.4. Case study – Analysis of an Saharan dust intrusion event with complementary techniques (Iași, România)**

Typically, Lidar data are validated with complementary techniques such as solar photometry, the Calipso Lidar system, and with theoretical models, namely MAP<sub>3</sub>D, DREAM, and HYSPLIT.

In this case study we use all the above-mentioned techniques and models to study the transport of Saharan dust on long distances and furthermore to check for possible influences on the local weather. Since the Saharan dust influences the radiative heat transfer via absorption, scattering or reflection, a net change in the energetic flux and solar wavelength reaching ground is expected. According to literature, atmospheric photosynthesis processes are also altered [36-38]. The presence of Saharan dust is indicated by data collected with solar photometry and from the theoretical models of aerosols dispersion, which make use of databases from various weather stations. The MAP<sub>3</sub>D model (detailed in Annex 2) is capable of providing daily prognosis for pollution in air (O<sub>3</sub>, NO, NO<sub>2</sub>, particles PM<sub>10</sub>) [39, 40]. At the core of the MAP<sub>3</sub>D sits the chemical model MM5/CHIMERE. In 2010, the MAP<sub>3</sub>D was implemented in Romania and has a spatial resolution of 15x15 km<sup>2</sup> [41, 42].

The measurements were performed during the month of July 2012. The month of July was chosen since the optical properties of aerosols vary during the transition between the warm and the cold seasons [43, 44], while July is in the middle of the warm season thus keeping the optical properties rather constant. Based on the data acquired from AERONET (Aerosol Robotics Network) and on the solar photometer installed in our laboratory (details given in Annex 2), we analyzed the Angstrom coefficient variation, and selected the data when Saharan dust inclusion where possible above the city of Iasi. Small values of the Angstrom coefficient imply an increase of the volumetric distribution of particle with a diameter larger than 1 μm, particles which can be called “coarse mode”. From Figure III.13, by tracking the variation of the Angstrom coefficient, there were extracted the periods of time in which such decreases were recorded. In this manner, the models HYSPLIT and DREAM validate the possibility of Saharan dust inclusion.

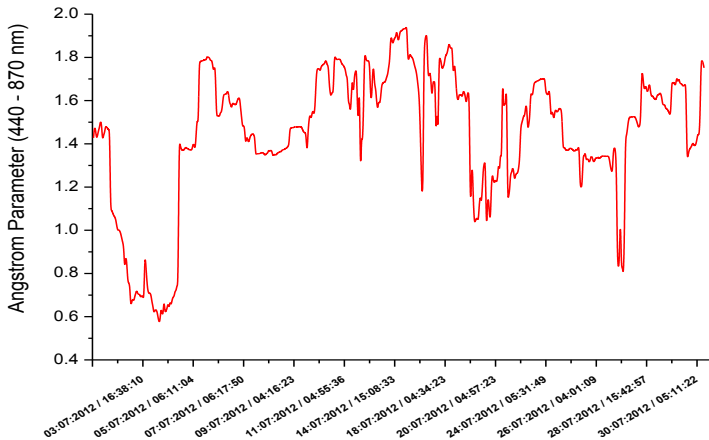


Figure III.13. The variation of the Angstrom coefficient in Iași, România – July 2013.

It is well known that in the area of the Iasi city, the urban and industrial aerosols are strongly influencing the atmosphere composition [45]. That is why it is of uttermost importance to correctly identify Saharan dust inclusion by also mapping qualitatively of particles like  $PM_{10}$ ,  $O_3$  and  $NO_2$  with the help of  $MAP_3D$ .

For the periods of time in which the Angstrom coefficient drops below 1.2, the HYSPLIT model is used to determine the days with Saharan dust inclusion (Figure III.14). The results obtained with the HYSPLIT model were validated by the DREAM model, confirming the presence of Saharan dust in the Iasi area (Fig. III.15).

Even if Saharan dust intrusions are noticed, the DREAM model indicated that the major contribution to aerosol concentration is given by the continental dust (urban and industrial). To obtain further information over the Saharan dust, the data has to come from higher atmospheric altitudes, where the continental dust contribution is negligible. With the DREAM model, Saharan the dust concentration is in the range of 0.05 - 0.5  $g/m^2$  above the measuring point.

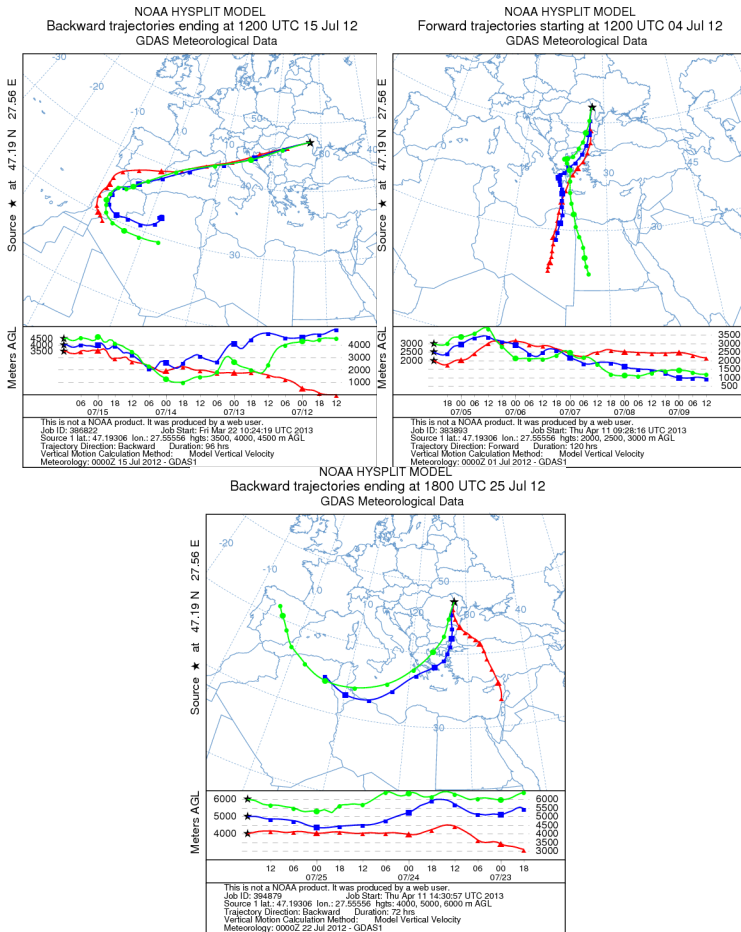


Figure III.14. Air mass trajectory resulting from the HYSPLIT model for (a) 4 July 2012, (b) 15 July 2012 and (c) 25 July 2012.

For the periods of time in which the DREAM model does not confirm the presence of Saharan dust, data collected from AERONET were analyzed. The optical parameters of the Saharan dust determined from the AERONET (the Angstrom coefficient ( $\alpha$ ), Single Scattering Albedo (SSA), LIDAR ratio ( $S_{AERONET}$ )) confirm the presence of Saharan dust: a sharp drop of the parameter  $\alpha$  from 1.4 to 0.5 and of the parameter  $S_{AERONET}$  from 50 sr to 30 sr [45].

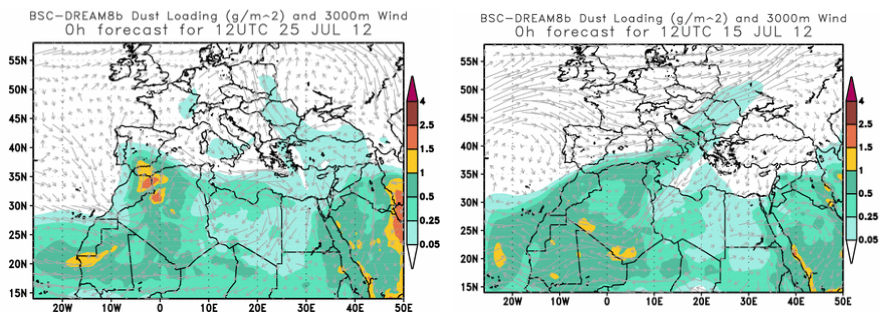


Figure III.15. Forecast given by the DREAM model for the days 15 and 25 of July 2012.

The results given by the DREAM model are used as input parameters for the MAP<sub>3</sub>D model (the data collected on the days 4, 15 and 25 of July 2012 – days with cloudy nebulosity, but with Saharan dust intrusion). The model MAP<sub>3</sub>D forecasts an increase in the PM<sub>10</sub> concentration. The concentration values are modeled for the troposphere and represent daily maximum values up to altitudes of 8000 m. The variation of the concentration over the entire month of July is given, indicating the increase over the entire tropospheric column.

During the days of 24<sup>th</sup> and 25<sup>th</sup> of July 2013, the MAP<sub>3</sub>D forecasted an increase in the PM<sub>10</sub> concentration while the DREAM model indicated a surface density characteristic to the Saharan dust (Fig. III.22). Additional details are provided by experimental data collected by CALIPSO (technical details given in Annex 2). In figure III.24 (a) the backscattering coefficient for the 25<sup>th</sup> of July (00.35 – 00.48 UTC) is given. The highlighted region indicates the feedback given by the interaction between the laser radiation and the atmospheric constituents. By calculating the optical parameters from the acquired Lidar signal, a classification of the aerosol types is given (Fig. III.16 (b)). From the experimental data provided by CALIPSO, it can be observed that the Saharan dust is visible up to 5000 m.

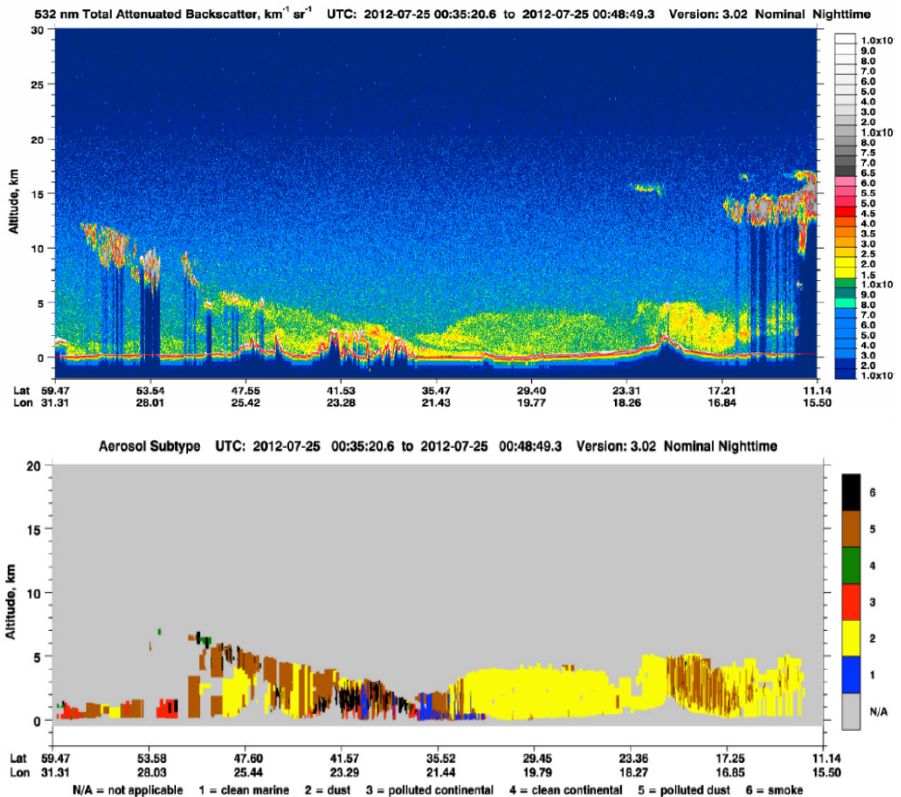
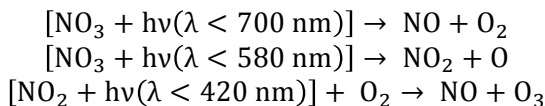


Figure III.16. (a) The backscattering Lidar coefficient 532 nm (CALIPSO) – 25 July 2012 and (b) aerosol classification based on the computation of optical parameters aided by Lidar signal.

The tropospheric ozone is influenced by repeats Sahran dust intrusions [46]. The Saharan dust absorbs wavelengths below 440 nm. The UV solar spectrum is reduced in the presence of Saharan dust while the IR solar spectrum is hardly modified. Strong changes in the ozone concentrations were not observed during the Saharan dust intrusions over the region of Iasi. The tropospheric ozone is influence by the solar spectrum as follows [47]:



From the chemical reactions, it can be seen that a variation of the ozone concentration implies a variation of the  $\text{NO}_2$  concentration.

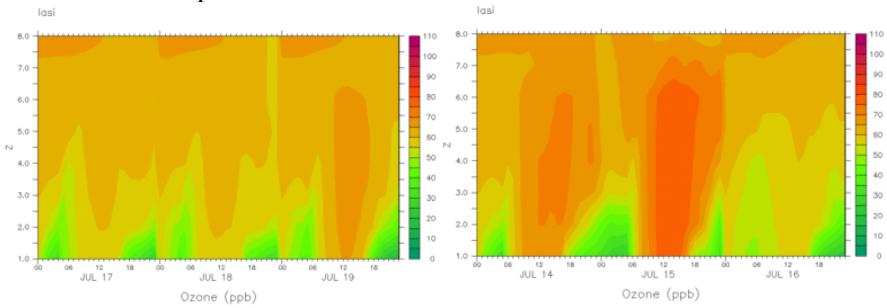


Figure III.17. Forecasted ozone concentration given by the MAP<sub>3</sub>D for the period 14 – 19 July 2012.

The three dimensional map of the ozone distribution is provided by the MAP<sub>3</sub>D model. In the Fig III.17 we can observe variations of the ozone concentration up to altitudes of 8000 m, variations attributed to known chemical reactions. We can conclude that the Saharan dust intrusions over the month of July 2012 did not influence the ozone concentration, most likely due to the low mineral dust concentration [48].

## Chapter IV – Conclusions and outlook

### *Personal contributions and novelties*

The technical improvements and the results presented in this doctoral dissertation are the result of an extensive research and development project started in 2007, namely the ROLINET project. It is my sincere hope that it will support future young and talented researchers to continue to improve techniques as exciting as Lidar, or use techniques to further deepen the understanding of climate changes.

During the doctoral studies (October 2010 – September 2013) the author of this thesis gained strong insight in the Physics of the Atmosphere and in the field of laser – atmosphere interaction, contributed at the development and the technical improvement of the <sup>ESY</sup>Lidar system and further implemented algorithms for pre-processing and processing of Lidar signals. Furthermore, using various techniques he showed how optical techniques can be used to diagnose the atmospheric composition with case studies including: mineral dust intrusion (Saharan dust), smoke detection (biomass burning), volcanic ash detection and others.

Some of the personal contributions include:

1. A new configuration <sup>ESY</sup>Lidar system was created, the on-axis mode. Although the results presented in this thesis were not acquired in the on-axis mode, the author demonstrated that this mode is a viable solution to diagnose the first hundreds of meters of atmosphere.

2. The alignment of the Lidar system has been improved by using micrometric positioning devices. The technical solution facilitated an immediate improvement in the Lidar system performance. Thus, a gain of 100 up to 150 m in altitude has been measured for complete overlap of the recorded signal. Additionally, the alignment procedure is fast, accurate, with least mechanical hysteresis, more stable, and easier to perform. The on-axis mode for the Lidar system greatly benefits this mechanical upgrade of the alignment system.

3. Reconfiguring the detection mode with only three detection channels (532 nm total, 532 nm parallel (in analog mode) and 532 nm perpendicular (in photon-counting mode)). From a scientific perspective, the introduction of this configuration to study polarization effects is maybe the most important development. In the community, it is becoming more obvious that polarized Lidar studies are shading

more and more light in the complex study of phenomena and processes occurring in the atmosphere.

4. Implementing routines for pre-processing and processing of the Lidar signals. The routines were developed in Labview with the assistance of the National Institute for Research and Development for Optoelectronics Magurele. These routines might enable the Romanian Network of Lidar systems to join larger worldwide networks, such as EARLINET. Such routines will standardize the data processing, data handling and sharing. It further allows operators to easier interpret the measured Lidar data.

5. Experimentally, several phenomena and processes for the Atmospheric Physics were shown: intrusions of mineral dust of Saharan origin, smoke detection originated from biomass burning, volcanic ash particle detection, study of the dynamics of the planetary boundary layer, etc.

6. From a scientific point of view, the author published 4 articles in ISI journals, 2 have been submitted for publications and 2 more are in preparation for submission. Furthermore, the author filled for a patent for the novelties brought to the Lidar system and published an article for the large audience in the magazine “Știință și tehnică” and another one in a conference proceedings journal. The author took part in a series of national and international conference and had 4 oral presentation and about 20 posters at conference held in Romania, Greece, Austria, The Czech Republic, Argentina, Switzerland, and others.

### ***Further development of and using the <sup>ESY</sup>Lidar system***

As a function of resources, manpower and financial, in a medium and/or long term the <sup>ESY</sup>Lidar system can be improved from a configuration point of view, thus enabling better performance while expanding the applicability of the system. The author noticed the following possible future research goals:

- In the on-axis configuration, photomultipliers with fast shutters or with gate must be included to avoid saturation effects in them.
- In the off-axis configuration, the reception module will be modified by replacing the afocal lens that collimates the backscattered radiation with a set of lenses able to focus the backscattered radiation for more wavelengths. At present, the Lidar system is capable to

receive only wavelengths of 532 nm, while the over wavelengths (355 nm, 387 nm and 607 nm) are not focused.

- In the off-axis mode, to achieve high quality polarized Lidar studies, a calibration of the degree of polarization must be introduced. According to the details presented in this doctoral dissertation, the method of calibrating at +/- 45 degrees proposed by Freundenthaler can be used. The polarizing module will be used for aerosols studies and as a complementary technique by the National System Anti-Hale, the Lidar system being capable of offering real time information regarding the water and ice content of clouds.

**This work was supported by the the European Social Fund in Romania, under the responsibility of the Managing Authority for the Sectoral Operational Programme for Human Resources Development 2007-2013 [grant POSDRU/107/1.5/S/78342].**

## Bibliography

- [1] C.C. Liu, C.C. Chen, T.N. Wu, C.Y. Yang, Association of brain cancer with residential exposure to petrochemical air pollution in Taiwan, *Journal of Toxicology and Environmental Health Part A* 71, 310-314; 2008.
- [2] W.B. Grant, Air pollution in relation to U.S. cancer mortality rates: an ecological study; likely role of carbonaceous aerosols and polycyclic aromatic hydrocarbons, *Anticancer Research* 29, 3537-3545, 2009.
- [3] S. Ștefan, *Fizica Aerosolului Atmosferic*, Editura All, 1998.
- [4] <http://mountpinatubo.net/Mount-Pinatubo-Eruption.html>
- [5] A. Robock, Volcanic Eruption, Mt. Pinatubo, The Earth system: physical and chemical dimensions of global environmental change, *Encyclopedia of Global Environmental Change*, John Wiley & Sons, Ltd, Chichester, 1, 737, 2002.
- [6] A. Muhlbauer, U. Lohmann, Aerosol-cloud interactions and the effects on orographic precipitation, 12th AMS Conference on Cloud Physics, Madison, USA, 10-14 July 2006.
- [7] E.H. Synge, *Philos. Mag.* 52, 1014-1020, 1930.
- [8] G. Fiocco, L.D. Smullins, *Nature* 199, 1275-1276, 1963.
- [9] R.M. Measures, *Laser Remote Sensing. Fundamentals and Applications*, Krieger Publishing Company, Malabar, Florida, 1992.
- [10] I. Matthias, Multiyear aerosol observations with dual wavelength Raman Lidar in the framework of EARLINET, *J. Geophys. Res.*, 109, D13203, 2004.
- [11] J.E. Barnes, D.J. Hoffman, Lidar measurements of stratospheric aerosol over Mauna Loa Observatory, *Geophys. Res. Lett.*, 24(15), 1923–1926, 1997.
- [12] <http://www.earlinet.org/>
- [13] <http://rolinet.inoe.ro/>
- [14] D. Nicolae, E. Carstea, I. Balin, A. Balanici, G. Picoulet, P. Ristori, Sistem MicroLIDAR Pentru Detectarea Profilelor Aerosolilor Atmosferici și a Norilor în 3D, *Buletinul Oficial de Proprietate Industrială, secțiunea Invenții*, nr. 11/2009.
- [15] O. Tudose, M.M. Cazacu, A. Timofte and I. Balin - ESYROLIDAR system developments for troposphere monitoring of aerosols and clouds properties, *Proceedings of SPIE - Remote Sensing*, 8177, 817716.1-817716.10, 2011.
- [16] S. Barth, R. Fizzano, C. van Nutt, J. Yeatts, Dichroic Filters On Flexible Polymer Film Substrates, US patent US 20070247720 A1, 2006.
- [17] M. Haupt, S. Miller, R. Sauer, K. Thonke, A. Mourran and M. Moeller, Breath figures: Self-organizing masks for the fabrication of photonic crystals and dichroic filters, *J. Appl. Phys.* 96, 3065, 2004.
- [18] M. Prelipceanu, O.S. Prelipceanu, O. Tudose, L. Leontie, B. Grimm, S. Schrader, Study of thermal conversion and patterning of a new soluble poly (p-phenylenevinylene) (PPV) precursor, *Materials Science in Semiconductor Processing* 10, 77, 2007.
- [19] J.M. Alvarez, M.A. Vaughan, C.A. Hostetler, W.H. Hunt, D.M. Winker. Calibration technique for polarization-sensitive Lidars. *J. Atmos. Ocean. Technol.* 23, 683–699, 2006.

- [20] [http://www.thorlabs.de/newgrouppage9.cfm?objectgroup\\_id=142](http://www.thorlabs.de/newgrouppage9.cfm?objectgroup_id=142)
- [21] M. Anni, G. Giglia, S. Patane, A. Arena, M. Allegrinic, R. Cingolania, Organic microcavities based on thermally evaporated TeOx-LiF dielectric mirrors, *Physica E* 13, 451 – 454, 2002.
- [22] M. E. Pollard, S. J. Pearce, R. Chen, S. Oo, M. D. B. Charlton, Polymer waveguide grating couplers for low-cost nanoimprinted integrated optics, *Proc. SPIE 8264, Integrated Optics: Devices, Materials, and Technologies XVI*, 826418, 2012.
- [23] M. Prelipceanu, O. Tudose, O.S. Prelipceanu, S. Schrader, K. Grytsenko, Study of oriented growth of oligofluorene–thiophene films onto aligned vacuum-deposited polytetrafluoroethylene layers, *Materials Science in Semiconductor Processing* 10, 24–35, 2007.
- [24] S. Stefan, D. Nicolae, M. Caian, *Secretele aerosolului atmosferic în lumina laserilor*, Ed. Ars Docendi, 2008.
- [25] Z. Wang, D. Liu, J. Zhou, Y. Wang, Experimental Determination of the Calibration Factor of Polarization-Mie Lidar, *Optical Review*, 16 (5), 566–570, 2009.
- [26] L. Belegante, Determinarea parametrilor optici ai aerosolilor folosind tehnici de detecție bazate pe împrăștierea Raman, PhD Thesis, Universitatea Politehnică București, 2011.
- [27] I. Balin, Measurement and analysis of aerosols, cirrus-contrails, water vapor and temperature in the upper troposphere with the Jungfraujoch LIDAR system, PhD Thesis, Ecole Polytechnique Federale du Lausanne, 2004.
- [28] O. Tudose, I. Balin, M. Cazacu, A. Bălănici, Configurație de sistem lidar multi-lungime de undă cu aliniere coaxială unică a emisiei laser”, cerere de brevet O.S.I.M. nr. înreg. U/00030/31.07.2013.
- [29] V. A. Kovalev, W. E. Eichinger, *Elastic LIDAR – Theory, Practice, and Analysis Methods*, Wiley InterScience a John Wiley & Sons Inc, 2004.
- [30] M. Tesche, A. Ansmann, D. Müller, D. Althausen, R. Engelmann, V. Freudenthaler, S. Groß, Vertically resolved separation of dust and smoke over Cape Verde using multiwavelength Raman and polarization Lidars during Saharan Mineral Dust Experiment 2008, *J. Geophys. Res.* 114, D13202, 2009.
- [31] C. Talianu, A. Nemuc, D. Nicolae, C.P. Cristescu. Dust event detection from LIDAR measurements, *U.P.B. Sci. Bull., Series A*, 69 (1), 57- 66, 2007.
- [32] S. Stefan, A. Nemuc, C. Talianu, D. Nicolae, V. Filip, J. Ciuciu, Dust Intrusion Influence on Atmospheric Boundary Layer Using Lidar Data, *Book Nucleation and Atmospheric Aerosols*, 1134-1138, 2007.
- [33] D.N. Nicolae, Tehnici LIDAR pentru caracterizarea aerosolilor din atmosfera joasă, PhD Thesis, Universitatea Politehnică București, 2006.
- [34] O. Tudose, R. Hertanu, O. Couach, I. Balin, Recent PBL investigations in iasi city area using the upgraded esyroLidar, 26th of International Lidar Radar Conference, Porto Heli, Greece, 2012.
- [35] O. Tudose, A. Balanici, O. Couach, I. Balin, Urban Planetary Boundary Layer investigations in cold season and complex topography in IASI city area using

- ESYROLIDAR, The General Assembly of the European Geosciences Union, EGU 2012, Viena, Austria, 2012.
- [36] M.M. Cazacu, A. Timofte, P. Mark, O. Tudose, S. Gurlui, D.O. Dorohoi, I. Balin, New mESYLIDAR system testing measurements: first results considering meteorological context in North East region of Romania, The General Assembly of the European Geosciences Union, EGU 2010, Viena, Austria, 2010.
- [37] O. Tudose, A. Boscornea, L. Buzdugan, M.M. Cazacu, D. Nicolae, Vertical and temporal variation of aerosol mass concentration at Magurele – Romania during EMEP/PEGASOS campaign, submitted to International Journal of Remote Sensing (nr. înreg. TRES-PAP-2013-0571).
- [38] M. Tesche, A. Ansmann, D. Müller, D. Althausen, I. Mattis, Vertical profiling of Saharan dust with Raman Lidars and airborne HSRL in southern Morocco during SAMUM. *Tellus B* 61, 144 – 164, 2008.
- [39] S. Nickovic, A. Papadopoulos, O. Kakaliagou, G. Kallos, Model for prediction of desert dust cycle in the atmosphere. *J. Geophys. Res.* 106, 18113–18129, 2001.
- [40] S. Ilavajhala, M.M. Wong, C.O. Justice, Fire Information for Resource Management System: Archiving and Distributing MODIS Active Fire Data, *IEEE Transactions on Geoscience and Remote Sensing*, 47 (1), 72-79, 2009.
- [41] G.A. D’Almeida, Desert aerosol characteristics and effects on climate. In: Leinen, M., Sarnthein, M (Eds.), *Palaeoclimatology and Palaeometeorology: Modern and Past Patterns of Global Atmospheric Transport*. NATO ASI Series C282, 311-338, 1987.
- [42] M. Escudero, S. Castillo, X. Querol, A. Avila, M. Alarcon, M.M. Viana, A. Alastuey, E. Cuevas, S. Rodriguez, Wet and dry African dust episodes over eastern Spain, *Journal of Geophysical Research* 110 (D18S08) 1-15, 2005.
- [43] R. Stull, *Meteorology for Scientists and Engineers*, third edition, 2010.
- [44] [http://quicklooks.inoe.ro/IASI-UAIC/photogallery.php?album\\_id=1](http://quicklooks.inoe.ro/IASI-UAIC/photogallery.php?album_id=1).
- [45] T. Ohde, H. Siegel, Impacts of Saharan dust and clouds on photosynthetically available radiation in the area of Northwest Africa, *Tellus B*, 64, 17160, 2012.
- [46] J.H. Seinfeld, S.N. Pandis, *Atmospheric Chemistry and Physics*, Wiley Interscience, 1998.
- [47] J.M. Haywood, J. Pelon, P. Ormenti, N. Bharmal, M. Brooks, Overview of the dust and biomass-burning experiment and African Monsoon multidisciplinary analysis special observing period, *J. Geophys. Res.*, 113, D00C17, 2008.
- [48] R. Frouin, H. Murakami, Estimating photosynthetically available radiation at the ocean surface from ADEOS-II global imager data. *J. Oceanogr.* 22 (3), 493–503, 2007.

## Personal contributions

### ISI articles:

1. **O. Tudose**, M.M. Cazacu, A. Timofte and I. Balin, <sup>ESYRO</sup>LIDAR system developments for troposphere monitoring of aerosols and clouds properties, Proceedings of SPIE - Remote Sensing, 8177, 16.1 - 16.10, 2011 (**citations: 1**).

### Citations:

1. Unga, Florin; Cazacu, Marius Mihai; Timofte, Adrian; et al., STUDY OF TROPOSPHERIC AEROSOL TYPES OVER IASI, ROMANIA, DURING SUMMER OF 2012, ENVIRONMENTAL ENGINEERING AND MANAGEMENT JOURNAL, Volume: 12, Issue: 2, Pages: 297-303, Published: FEB 2013.

2. M. Prelipceanu, O.S. Prelipceanu, **O. Tudose**, L. Leontie, B. Grimm, S. Schrader, Study of thermal conversion and patterning of a new soluble poly (p-phenylenevinylene) (PPV) precursor, Materials Science in Semiconductor Processing 10, 77, 2007 (**impact factor 1,33; relative influence score 0.76, citations 8**).

### Citations:

1. Heydari, Reza; Tahamipour, Batool; Torbati, Niloofar Akbarzadeh; et al., One-Pot Synthesis and X-Ray Structure of New, Stable Tetrahydropyrrolo [1,2-a][1,10]phenanthrolines with Four Diastereoisomeric Centers, SYNTHETIC COMMUNICATIONS, Volume: 43, Issue: 15, Pages: 2031-2041, Published: AUG 2013.

2. Heydari, Reza; Tahamipour, Batool, Highly regioselective synthesis of dicyano-8a,10,11-trihydropyrrolo [1,2-a][1,10]phenanthrolines via a domino-Knoevenagel-cyclization, CHINESE CHEMICAL LETTERS Volume: 22, Issue: 11, Pages: 1281-1284, Published: NOV 2011.

3. Al-Hariri, Lara A.; Zheng, Lianqing; Yang, Wei; et al., Thermal Elimination of Precursors to Poly(phenylenevinylene) with a Macrocounterion versus a Small Counterion: A Coordinated Experimental and Simulation Study, MACROMOLECULES, Volume: 44, Issue: 17, Pages: 6663-6668, Published: SEP 2011.

4. Supangat, A.; Zhou, X. J.; Belcher, W.; et al., Chemical vapour deposition of poly(p-phenylenevinylene) nanofilms for use in organic photovoltaics, MATERIALS RESEARCH INNOVATIONS, Volume: 15, Supplement: 2, Pages: 18-20, Published: AUG 2011.

5. Tahamipour, Batool; Heydari, Reza; Torbati, Niloofar Akbarzadeh; et al., Diastereoselective synthesis and X-ray structure of new stable dicyano (8aRS, 10SR, 11SR)-9,9-dicyano-10-aryl-11-benzoyl-8a, 9,10,11-tetrahydropyrrolo[1,2-a][1,10]phenanthrolines, JOURNAL OF CHEMICAL RESEARCH, Issue: 6, Pages: 329-332, Published: JUN 2011.

6. Muroyama, Masakazu; Saito, Wataru; Yokokura, Seiji; et al., Maskless Patterning of Vapor-Deposited Photosensitive Film and its Application to Organic

Light-Emitting Diodes, JAPANESE JOURNAL OF APPLIED PHYSICS, Volume: 50, Issue: 4, Special Issue: SI, Article Number: 04DK07, Published: APR 2011.

7. Al-Hariri, Lara A.; Schlenoff, Joseph B., Macro-counterions in a precursor to poly(phenylene vinylene): Toward defect-free luminescent films, POLYMER, Volume: 51, Issue: 14, Pages: 2993-2997, Published: JUN 2010.

8. Kim, Yuna; Yun, Chijung; Jadhav, Parashuram; et al., Emissive pattern formation by the photoreaction of poly(p-phenylene vinylene), CURRENT APPLIED PHYSICS Volume: 9, Issue: 5, Pages: 1088-1092, Published: SEP 2009.

3. M. Prelipceanu, **O. Tudose**, O.S. Prelipceanu, S. Schrader, K. Grytsenko, Study of oriented growth of oligofluorene–thiophene films onto aligned vacuum-deposited polytetrafluoroethylene layers, Materials Science in Semiconductor Processing 10, 24–35, 2007 (**impact factor 1,33; relative influence score 0.76, citations 5**).

#### **Citations:**

1. Rahachou, A. V.; Rogachev, A. A.; Yarmolenko, M. A.; et al., Molecular structure and optical properties of PTFE-based nanocomposite polymer-metal coatings, APPLIED SURFACE SCIENCE Volume: 258, Issue: 6, Pages: 1976-1980, Published: JAN 2012.

2. Jiang, Shidong; Qian, Hualei; Liu, Wei; et al., Vapor Phase Epitaxy of Perylo[1,12-b,c,d]thiophene on Highly Oriented Polyethylene Thin Films, MACROMOLECULES Volume: 42, Issue: 23, Pages: 9321-9324, Published: DEC 2009.

3. Rogachev, Alexander A.; Tamulevicius, Sigitas; Rogachev, Alexander V.; et al., The structure and molecular orientation of polytetrafluoroethylene coatings deposited from active gas phase, APPLIED SURFACE SCIENCE Volume: 255, Issue: 15, Pages: 6851-6856, Published: MAY 2009.

4. Liu, Shuhong; Wang, Wechung Maria; Briseno, Alejandro L.; et al., Controlled Deposition of Crystalline Organic Semiconductors for Field-Effect-Transistor Applications, ADVANCED MATERIALS Volume: 21, Issue: 12, Pages: 1217-1232, Published: MAR 2009.

5. Grytsenko, K. P., Vacuum evaporation-deposited polytetrafluoroethylene films: Growth mechanism, properties, and applications, RUSSIAN JOURNAL OF GENERAL CHEMISTRY Volume: 79, Issue: 3, Pages: 642-656, Published: MAR 2009.

4. A. Covășnianu, **O. Tudose**, Airborne LIDAR data and GIS technique outputs over Romanian Danube plain with a special attention on geomorphology, Carpathian Journal of Earth and Environmental Sciences, 8 (1), 117 – 126, 2013 (**impact factor 1,49; relative influence score 0.08**).

### **Submitted ISI articles:**

1. **O.G. Tudose**, M.M. Cazacu, Aerosol characteristics under Saharan dust loading above Iasi, Romania during July 2012, trimis spre publicare la Revista de Chimie.
2. **O.G. Tudose**, A. Boscornea, L. Buzdugan, M.M. Cazacu, D. Nicolae, Vertical and temporal variation of aerosol mass concentration at Magurele – Romania during EMEP/PEGASOS Campaign, submitted to International **Journal of Remote Sensing**.

### **Other publications:**

1. **O.G. Tudose** - <sup>mESY</sup>LIDAR, un instrument potrivit pentru monitorizarea atmosferei și a gradului de poluare a acesteia, Science&Technique (ISSN: 1220-6555), 2013.

### **Proceedings of the conferences:**

1. M. Cazacu, I. Vetres, P. Ristori, P. Mark, **O.G. Tudose**, D. Nicolae, D. Dorohoi, I. Balin – <sup>mESY</sup>LIDAR – a new up-gradable and versatile LIDAR configuration for 3D monitoring of atmospheric aerosols, clouds and water vapor within ROLINET project, 3<sup>rd</sup> International Workshop on Optoelectronic Techniques for Environmental Monitoring – OTEM 2009, 30 Septembrie – 2 Octombrie 2009.

### **Oral presentations:**

1. **O.G. Tudose**, D.O. Dorohoi and I. Balin – Air monitoring in Iasi area by spectroscopic techniques, 31<sup>st</sup> European Congress on Molecular Spectroscopy - EUCMOS 2012, Cluj Napoca, Romania, August 2012.
2. I. Balin, **O.G. Tudose**, O. Couach and D. Nicolae - Remote sensing of the atmosphere: Monitoring air pollution - understanding climate changing, 4th International Workshop on Optoelectronic Techniques for Environmental Monitoring – OTEM 2011, Bucuresti, Romania, Septembrie 2011.
3. M.M. Cazacu, **O.G. Tudose**, I. Balin, <sup>mESY</sup>LIDAR system developments for troposphere monitoring of aerosols and clouds properties, 8<sup>th</sup> Swiss Geoscience Meeting, Hot and Cold: Extreme Climates in Space and Time, Fribourg, Switzerland, Noiembrie 2010.
4. M. Cazacu, I. Vetres, P. Ristori, P. Mark, **O.G. Tudose**, D. Nicolae, D. Dorohoi, I. Balin – <sup>mESY</sup>LIDAR – a new up-gradable and versatile LIDAR configuration for 3D monitoring of atmospheric aerosols, clouds and water vapor within ROLINET project, 3<sup>rd</sup> International Workshop on Optoelectronic Techniques for Environmental Monitoring – OTEM 2009; Bucuresti, Romania, Septembrie 2009.

### **Posters:**

1. **O.G. Tudose** - LIDAR technique: a central puzzle piece to build an integrated observation - modelling approach for air mass aerosols concentration evaluation, The General Assembly of the European Geosciences Union, EGU 2013, Viena, Austria, Aprilie 2013.

2. **O.G. Tudose**, I. Balin - <sup>ESY</sup>LIDAR - a new powerful configuration for 3D monitoring of tropospheric aerosols and clouds, European Exhibition of Creativity and Innovation (EUROINVENT), Iasi, Romania, 9-11 May 2013.
3. **O.G. Tudose**, I. Balin, A. Balanici - 3D ATMOSPHERIC POLLUTION EXPERIMENTAL APPROACH IN NORTH EAST REGION OF ROMANIA, "Environmental Legislation, Safety Engineering and Disaster Management", 25-27 octombrie 2012, Cluj Napoca, Romania.
4. **O.G. Tudose**, A. Boscornea, L. Buzdugan, M.M. Cazacu, D. Nicolae - VERTICAL AND TEMPORAL VARIATION OF AEROSOL MASS CONCENTRATION AT BUCHAREST DURING EMEP/PEGASOS CAMPAIGN, "Environmental Legislation, Safety Engineering and Disaster Management", 25-27 octombrie 2012, Cluj Napoca, Romania
5. **O.G. Tudose**, R. Hertanu, A. Balanici, O. Couach, I. Balin - <sup>ESYRO</sup>LIDAR investigation of Planetary Boundary Layer over Iasi – Romania urban areas, The 9<sup>th</sup> International Symposium on Tropospheric Profiling (ISTP), L'Aquila, Italy, September 3<sup>th</sup>-7<sup>th</sup>, 2012
6. **O.G. Tudose**, D.O. Dorohoi, I. Balin - OPTICS OF LIDAR SYSTEM USED FOR SPECTROSCOPIC MONITORING OF AIR POLLUTION, European Congress on Molecular Spectroscopy", 26 - 31 August, 2012, Cluj-Napoca, Romania.
7. **O.G. Tudose**, D.O. Dorohoi, I. Balin - INVESTIGATION OF ATMOSPHERIC POLLUTION BY LIDAR AND OTHER SPECTROSCOPIC TECHNIQUES, 9<sup>th</sup> International Conference On Physics Of Advanced Materials (ICPAM-9), Iasi, septembrie 2012.
8. **O.G. Tudose**, R. Hertanu, O. Couach, I. Balin - Recent PBL investigations in Iasi city area using the upgraded <sup>esyro</sup>Lidar, 26<sup>th</sup> of International Lidar Radar Conference, Porto Heli, Greece, Iunie 2012.
9. **O.G. Tudose**, A. Balanici, O. Couach and I. Balin - Urban Planetary Boundary Layer investigations in cold season and complex topography in IASI city area using <sup>ESYRO</sup>LIDAR, The General Assembly of the European Geosciences Union, EGU 2012, Viena, Austria, Aprilie 2012.
10. **O.G. Tudose**, M.M. Cazacu, A. Timofte and I. Balin - <sup>ESYRO</sup>LIDAR system developments for troposphere monitoring of aerosols and clouds properties, Poster 8177-55, SPIE - Remote Sensing, Prague, Septembrie 2011.
11. **O.G. Tudose**, M.M. Cazacu, A. Timofte, I. Balin, D. Nicolae – Performances analysis of a new powerful LIDAR configuration for 3D monitoring of tropospheric aerosols and clouds, The General Assembly of the European Geosciences Union, EGU 2011, Viena, Austria, Aprilie 2011.
12. I. Balin, M. Cazacu, **O.G. Tudose**, C. Mahalu, S. Gurlui, D. Costin, V. Ristici, I. Vetres, D. Nicolae, State of the art of the LIDAR systems development for the Romanian Lidar national NETWORK ROLINET, 4th International Workshop on Optoelectronic Techniques for Environmental Monitoring – OTEM 2010, Cluj-Napoca, Romania; Octombrie 2010.

13. M.M. Cazacu, **O.G. Tudose**, V. Ristici, D. Nicolae, I. Balin, Integration of a UV-VIS-NIR Nd:YAG laser system in a new LIDAR system, International Student Workshop on Laser Applications 2010, ISWLA'10, Bran, Romania, Mai 2010.
14. M.M. Cazacu, A. Timofte, **O.G. Tudose**, D. Dimitriu, S. Gurlui, I. Balin – <sup>mESY</sup>LIDAR – A new configuration for 3D monitoring of atmospheric aerosols and clouds, A XXXIX-a Conferinta Nationala Fizica si Tehnologice Educationale Moderne, Iasi, Romania, Mai 2010.
15. M.M. Cazacu, A. Timofte, P. Mark, **O.G. Tudose**, S. Gurlui, D.O. Dorohoi, I. Balin – New <sup>mESY</sup>LIDAR system testing measurements: first results considering meteorological context in North East region of Romania, The General Assembly of the European Geosciences Union, EGU 2010, Viena, Austria, Mai 2010.
16. A. Covasnianu, **O.G. Tudose**, M.M. Cazacu, I. Nichersu, M. Memier, I. Balin - R.E.E.L.D. (Economical and Ecological Reconstruction of the Danube Flood Plain) Campaign: airborne LIDAR data and GIS technique outputs, The General Assembly of the European Geosciences Union, EGU 2010, Viena, Austria, Mai 2010.
17. M. M. Cazacu, P. Ristori, **O.G. Tudose**, A. Balanici, D. Nicolae, V. Ristici, D. Balin, I. Balin, <sup>mESY</sup>LIDAR: a new cost-effective powerful lidar configuration for tropospheric aerosols and clouds investigations, 5<sup>th</sup> Workshop Lidar Measurements in Latin America, Buenos Aires, Argentina, Decembrie 2009.
18. M.M. Cazacu, P. Ristori, **O.G. Tudose**, A. Balanici, D. Nicolae, V. Ristici, D. Balin, I. Balin – <sup>mESY</sup> LIDAR - a new cost-effective, versatile and powerful lidar configuration for tropospheric aerosols, clouds and water vapor investigations, The General Assembly of the European Geosciences Union, EGU 2009, Viena, Austria, Aprilie 2009.